



# JRC TECHNICAL REPORT

## Radionuclide Metrology

*Confidence in radioactivity  
measurements*

Stefaan Pommé

2022



This publication is a Technical report by the Joint Research Centre (JRC), the European Commission's science and knowledge service. It aims to provide evidence-based scientific support to the European policymaking process. The scientific output expressed does not imply a policy position of the European Commission. Neither the European Commission nor any person acting on behalf of the Commission is responsible for the use that might be made of this publication. For information on the methodology and quality underlying the data used in this publication for which the source is neither Eurostat nor other Commission services, users should contact the referenced source. The designations employed and the presentation of material on the maps do not imply the expression of any opinion whatsoever on the part of the European Union concerning the legal status of any country, territory, city or area or of its authorities, or concerning the delimitation of its frontiers or boundaries.

#### Contact information

Name: Stefaan Pommé  
Address: Joint Research Centre – JRC, Retieseweg 111, B-2440 Geel, Belgium  
Email: stefaan.pomme@ec.europa.eu  
Tel.: +32 14 571 289

#### EU Science Hub

<https://ec.europa.eu/jrc>

JRC129308

EUR 31134 EN

PDF

ISBN 978-92-76-54093-9

ISSN 1831-9424

doi: 10.2760/666973

Geel: European Commission, 2022

© European Atomic Energy Community, 2022



The reuse policy of the European Commission is implemented by the Commission Decision 2011/833/EU of 12 December 2011 on the reuse of Commission documents (OJ L 330, 14.12.2011, p. 39). Except otherwise noted, the reuse of this document is authorised under the Creative Commons Attribution 4.0 International (CC BY 4.0) licence (<https://creativecommons.org/licenses/by/4.0/>). This means that reuse is allowed provided appropriate credit is given and any changes are indicated. For any use or reproduction of photos or other material that is not owned by the EU, permission must be sought directly from the copyright holders.

All content © European Atomic Energy Community, 2022

How to cite this report: S. Pommé, *Radionuclide Metrology – Confidence in radioactivity measurements*, EUR 31134 EN, European Commission, Geel, 2022, ISBN 978-92-76-54093-9, doi:10.2760/666973, JRC129308.

## Contents

1	Introduction.....	3
2	A common measurement system for activity.....	4
2.1	Primary standardisation of activity.....	4
2.2	Dissemination of the becquerel.....	5
2.3	Mutual recognition of national standards.....	5
2.4	A measure of equivalence.....	6
2.5	Meta-analysis of equivalence .....	7
3	Primary standardisation at the JRC.....	9
3.1	Joint Research Centre .....	9
3.2	Source preparation.....	9
3.3	Large Pressurised Proportional Counter.....	10
3.4	$4\pi \beta\gamma$ coincidence counter.....	11
3.5	$4\pi \gamma$ counter.....	14
3.6	CsI(Tl) sandwich spectrometer.....	15
3.7	Counting at a defined solid angle .....	16
3.8	Liquid Scintillation Counters.....	17
3.9	PomPlot of key comparisons.....	18
3.10	Secondary standardisation.....	21
4	Nuclear decay data.....	22
4.1	Need for reliable decay data.....	22
4.2	Intermediate half-life measurements.....	22
4.3	Short and long half-life measurements.....	24
4.4	Alpha-particle emission probabilities.....	25
4.5	Internal Conversion Coefficients.....	28
4.6	Gamma-ray intensities .....	30
4.7	Cross sections.....	31
4.8	$k_0$ factors .....	31
4.9	Fission product yields.....	32
5	The time dimension .....	34
5.1	The exponential-decay law .....	34
5.2	The 5 <sup>th</sup> force .....	34
5.3	Radiochronometry.....	36
5.4	Renewal processes.....	38
5.5	Counting statistics.....	39
6	Epilogue.....	43
7	Conclusions.....	44
8	References.....	45

9 List of figures .....	56
-------------------------	----

## Acknowledgements

Dr. Dr. Stefaan Pommé received the 2020 Hevesy Medal Award in recognition of his worldwide leadership in radioactivity measurements at the highest level of accuracy, providing absolute standards, accurate decay data, and innovative methods. The George Hevesy Medal Award is the premier international award of excellence in radioanalytical and nuclear chemistry. It is named after George de HEVESY (1885-1966) who received the Nobel Prize for Chemistry in 1943 for his work on the use of isotopes as tracers in the study of chemical processes. The George Hevesy Medal is awarded to an individual in recognition of excellence through outstanding, sustained career achievements in the fields of pure as well as applied nuclear and radiochemistry, in particular applications to nuclear analytical chemistry. This life-time achievement award pertains to the author's career in fission research at the Ghent University and the JRC, neutron activation analysis and gamma-ray spectrometry at the Belgian Nuclear Research Centre, and eventually primary standardisation of activity and accurate decay data measurements at the JRC.

The Radionuclide Metrology team of the JRC performs reference measurements of activity and nuclear decay characteristics in support of the common measurement system for radioactivity, as stipulated in Article 8 of the Euratom Treaty. Primary standardisations of activity performed at the JRC and National Metrology Institutes are used at a global scale to establish radioactivity measurements in a traceable manner to the SI-derived unit becquerel. The accurate decay data allow routine laboratories to convert detected emission rates into activity values. The author gratefully acknowledges the substantial input from past and present colleagues and external collaborators.

### ANNOUNCEMENT OF THE 2020 HEVESY MEDAL AWARDEE

The 2020 Hevesy Medal Award Selection Panel (HMASP-2020) is pleased to announce that **Dr. Stefaan POMMÉ** (Stefaan.POMME@ec.europa.eu) of the European Commission, Joint Research Centre (JRC) in Geel, Belgium has been selected to receive the 2020 Hevesy Medal Award (HMA-2020) in recognition of his worldwide leadership in radioactivity measurements at the highest level of accuracy providing absolute standards, accurate decay data, and innovative methods.



## **Abstract**

Radionuclides, whether naturally occurring or artificially produced, are readily detected through their particle and photon emissions following nuclear decay. Radioanalytical techniques use the radiation as a looking glass into the composition of materials, thus providing valuable information to various scientific disciplines. Absolute quantification of the measurand often relies on accurate knowledge of nuclear decay data and detector calibrations traceable to the SI units. Behind the scenes of the radioanalytical world, there is a small community of radionuclide metrologists who provide the vital tools to convert detection rates into activity values. They perform highly accurate primary standardisations of activity to establish the SI-derived unit becquerel for the most relevant radionuclides, and demonstrate international equivalence of their standards through key comparisons. The trustworthiness of their metrological work crucially depends on painstaking scrutiny of their methods and the elaboration of comprehensive uncertainty budgets. Through meticulous methodology, rigorous data analysis, performance of reference measurements, technological innovation, education and training, and organisation of proficiency tests, they help the user community to achieve confidence in measurements for policy support, science, and trade. The author dedicates the George Hevesy Medal Award 2020 to the current and previous generations of radionuclide metrologists who have devoted their professional lives to this noble endeavour.

## 1 Introduction

The discovery of spontaneous radioactive decay of unstable nuclei has altered the way that the atomic structure was perceived. No longer was the atom indivisible and immutable, and a suite of subatomic particles has been identified since then. Fundamental research entered into the abstract world of quantum mechanics to describe non-intuitive phenomena at atomic and subatomic levels. Through interactions with particles, stable atoms could be transformed into manmade radionuclides. However, their radioactive decay remained a random process, governed by invariable nuclide-specific decay rates. Vast amounts of energy could be unleashed from nuclear reactions. The emitted radiation interacting with matter offered possibilities for powerful nuclear measurement techniques, as well as medical applications in imaging, diagnostics, and therapy. The risk of physical harm through radiation exposure of the human body has always been the downside of this phenomenon.

The nuclear dimension offered new possibilities and challenges in analytical chemistry. New radioisotopes were formed and characterised. Some of these nuclides were used as tracers to follow natural processes, such as element uptake in biological entities or oceanographic currents. The radioanalytical techniques and their applications are quite diverse, and touch many fields of research, including biology, hydrology, geology, cosmology, archaeology, atmospheric sciences, health protection, pharmacology, chemistry, physics, and engineering. Radioactivity plays a particular role in establishing a measure of time, as the exponential-decay law predicts the relationship between the amounts of decaying atoms and their progeny as a function of time. Determination of this ratio allows age dating of materials, for example for geochronology or nuclear forensics.

Thousands of radionuclides have been investigated for their decay properties, not only as a looking glass to the interior of the atom, but also as a means for their identification and quantification through radioanalytical techniques. Hundreds of nuclides are of particular importance in the context of human health, medical applications, nuclear energy production, environmental monitoring, or astrophysics. Acquiring reliable and precise data on decay properties, such as decay modes, branching ratios, photon and particle emission probabilities and energies, half-lives, as well as cross section data for nuclear production processes is a painstaking task which is still far from completion and perfection. Quite rare is the availability of primary standards for the activity of relevant radionuclides, to which the detection efficiency of a measurement setup could be calibrated.

Behind the vast scene of nuclear science and its many applications, stands a small international community of radionuclide metrologists who lay the foundations for a common measurement system for radioactivity. They are at the apex of the metrology pyramid, providing the most accurate measurements of activity by means of primary standardisation techniques. Through key comparisons of their standards, they demonstrate international equivalence and realise the SI-derived unit becquerel (Bq). Through secondary standardisation, the world is provided with calibration sources to establish SI-traceability for all radioactivity measurements. Radionuclide metrology laboratories provide the tools needed to convert a count rate in a nuclear detector into an SI-traceable activity: certified radioactive sources for calibration, accurate half-life values, emission probabilities of various types of radiation (x rays, gamma rays, alpha particles, conversion electrons, Auger electrons), and evaluated decay schemes of the most important radionuclides. They provide sound methodology for the user communities, and are proactive in developments and quality control of personalised nuclear medicine.

This paper is part of the George Hevesy Medal Award 2020 lecture at the 12th International Conference on Methods and Applications of Radioanalytical Chemistry (MARC XII) held on April 3-8, 2022 in Kailua-Kona, Hawaii. It contains personal reflections of the author on highlights in his career and pays tribute to the hundreds of collaborators who helped to shape his contributions in the world of radionuclide metrology, neutron activation analysis, and experimental fission research.

## **2 A common measurement system for activity**

### **2.1 Primary standardisation of activity**

The measurand of an activity measurement is the expectation value at a reference time of the number of radioactive decays per second of a particular radionuclide in a material. It is expressed in the SI-derived unit becquerel, which corresponds to 1 aperiodic decay per second. Primary standardisation of radioactivity pertains to the absolute measurement of nuclear decays occurring per unit time. What is considered a primary method for the realisation of the unit becquerel differs from one radionuclide to another, depending on how their excess energy is emitted in the form of radiation. In this respect, the standardisation of activity entails a higher work load than for other SI units, since it has to be executed for each radionuclide of interest separately, by means of a selection of suitable techniques under specific conditions.

Ideally, a primary standardisation method for a particular radionuclide is designed in such a way that (i) its calibration is based on basic physical principles, not on other radioactivity measurements, (ii) its result is independent of the various nuclear decay data and their associated uncertainties, (iii) it is under statistical control, i.e. all main sources of uncertainties are identified and quantified, and (iv) the total uncertainty of the result is reduced to a minimum. In practice, a method is called primary when it has a combination of the above characteristics which is competitive with the best methods available for the specific radionuclide. The transparency and completeness of the uncertainty budget as well as the accuracy of the measurement result are important criteria.

The radionuclide metrology community has published two special issues of *Metrologia*, one explaining the state-of-the-art of measurement techniques used in standardisation of activity [1], and another elaborating in detail the uncertainty components involved in using them [2]. Primary techniques can be subdivided into high-geometry methods that aim at 100% detection efficiency, defined-solid-angle counting methods which extrapolate the total activity from a measurement of a geometrically well-defined fraction of emissions, and coincidence counting methods which inherently return detection efficiencies from coincidence rates in multiple detectors [3]. All counting methods require excellent compensation for count losses resulting from pulse pileup and system dead time, which is generally achieved by live-time counting and imposing a comparably long dead time of a known type (extending or non-extending) when registering a count [4]. Most of the significant sources of uncertainty are known and quantifiable, yet presenting a complete uncertainty budget remains a challenge that may require extensive modelling [5].

Whereas one can standardise the activity of a particular mononuclidic source, e.g. in the form of a radioactive deposit on an ultra-thin polymer foil, the realisation of the becquerel is generally performed for a radionuclide in acidic solution and expressed as an activity per unit mass of the solution, in kBq g<sup>-1</sup>. Source preparation involves quantitative dispensing of aliquots of the solution onto a substrate, the amounts being determined by weighing of the dispenser bottle on a calibrated microbalance before and after drop deposition [6]. The timing and duration of each measurement need to be accurately recorded by means of a clock synchronised to coordinated universal time (UTC), so that the results from activity measurements can be stated at a fixed reference time. The clock frequency of timing chips in live-time modules is verified by comparison with disseminated reference frequency signals. A standardisation of activity therefore requires SI-traceability to the unit of mass as well as time and frequency.

## **2.2 Dissemination of the becquerel**

Metrology is key to unlocking the benefits as well as controlling the harm of ionising radiation, in view of the omnipresence and widespread use of radioactivity in numerous applications. The user community needs calibration sources to determine the efficiency of their detectors, so that count rates can be converted into activity values. The calibration sources are traceable to the primary standards through a chain of direct comparisons, each step involving an additional uncertainty propagation. Secondary standards in radioactivity are usually pure solutions carrying a single radionuclide, which are measured relative to a corresponding primary standard in the same geometry in a transfer instrument. Common practice is the use of a stable, re-entrant pressurised gas ionisation chamber enclosing a few grams of solution contained in a sealed glass ampoule [7,8]. The activity ratio of the secondary to primary standard follows directly from the ratio of their ionisation currents. Calibration sources from a secondary standard can be produced from quantitative aliquots of the solution.

Traceability is a vertical comparison scheme that connects activity measurements with a particular standard [9]. Ionisation chambers are also used as hospital calibrators for short-lived radionuclides to be administered to patients for diagnosis and therapy. Their calibration factors are usually provided by the manufacturer, based on a particular traceability chain. In proficiency tests, the calibration factors for different geometries can be compared to an independent secondary standardisation by a metrology institute [10,11]. Recently, the first international proficiency test was held for combinations of nuclides which can be used together as theragnostic pairs [11]. Such actions bring quantitative personal medicine closer to practice.

## **2.3 Mutual recognition of national standards**

International collaboration in nuclear metrology is driven by common issues, such as trade, healthcare, environmental stewardship, nuclear security, and science [12,13]. The common radioactivity measurement system is promoted by the Consultative Committee for Ionizing Radiation (CCRI), which advises the International Committee for Weights and Measures (CIPM) in its task of promoting world-wide uniformity in units of measurement. The CIPM operates under the auspices of the General Conference (CGPM), which takes all the major decisions related to the propagation and improvement of the SI. It is the Key Comparison Working Group of section II of the CCRI, KCWG(II), that discusses the needs for establishing the SI-derived unit becquerel and advises on organising Key Comparisons (KCs) of radioactivity standards among the National Metrology Institutes (NMIs).

The Mutual Recognition Arrangement (CIPM MRA) is the framework through which NMIs demonstrate the international equivalence of their Calibration and Measurement Capabilities (CMCs), which they make publicly available to the user community through the key comparison database (KCDB) [14]. As a result of this horizontal comparison scheme, a common definition of the becquerel is established and users are not confined within state borders to seek particular radioactivity standards. Two approaches are used for comparison exercises. In the first approach, samples of a single radioactive solution are distributed to all participating laboratories and the results of their activity measurements are directly compared. The alternative approach is for NMIs to individually submit a standardised solution for indirect comparison through one of three transfer instruments operated by the International Bureau of Weights and Measures (BIPM): the SIR, SIRTI and ESIR (Fig. 1).



*Figure 1: The SIR, SIRTI, and ESIR activity transfer instruments operated by the Ionizing Radiation Department of BIPM for demonstrating equivalence of the SI-derived unit becquerel.*

The original International Reference System (SIR) [15,16], introduced at the BIPM in 1976, is based on two stable ionisation chambers in which glass ampoules containing standardised solutions of mononuclidic gamma-ray emitters are measured. The ratio between the ionisation current and the NMI-supplied activity is documented, with corrections for radioactive decay and impurities. This so-called ‘equivalent activity’ can be compared directly among NMIs in the present as well as in the past. Since 2007, a traveling NaI(Tl) well detector called SIRTI [17] was put into use as transfer instrument for short-lived positron emission tomography (PET) nuclides ( $^{99m}\text{Tc}$ ,  $^{18}\text{F}$ ), thus bringing the reference to remote places out of reach of the SIR. A further extension of the SIR being developed at the BIPM, the ‘extended SIR’ or ESIR [18], uses triple-to-double coincidence counting in a liquid scintillation cocktail to compare activities of pure beta or alpha emitters not accompanied by significant gamma-emissions.

## 2.4 A measure of equivalence

Equivalence of standards does not imply equality, but it ensures statistical consistency in the presence of measurement uncertainty [8]. The laboratories report extensive uncertainty budgets, addressing each potential source of error and associated uncertainty estimate, adhering to the rules of the Guide to the Expression of Uncertainty in Measurement (GUM) [19] and the International Vocabulary of Metrology (VIM) [20] issued by the Joint Committee for Guides in Metrology (JCGM). Since there is no objective arbiter in interlaboratory comparisons at the highest level of metrological accuracy, the Key Comparison Reference Value (KCRV) is a consensus value derived from the massic activity values provided by the participating laboratories. The ‘Degree of Equivalence’ compares the difference between the laboratory value and the KCRV with the expanded uncertainty of this difference [21].

For decades, the KCRV was calculated as an arithmetic mean, which acknowledges an equal weight among NMIs, but lacks efficiency at a scientific level by ignoring differences in the stated uncertainties. In May 2013, Section II of the CCRI was the first Consultative Committee that succeeded in adopting a weighting method, based on the ‘Power-Moderated Mean’ (PMM) [21,22,23]. In a trade-off between efficiency and robustness of the mean, the PMM uses an algorithm that applies statistical weighting of data when the stated uncertainties are realistic, yet moderates the weighting when they are not realistic and provides a criterion to identify extreme data eligible for rejection on statistical grounds. The PMM is easy to implement [24] and simulations show that it provides a robust mean and uncertainty, irrespective of the level of consistency of the data set. As a result of using the PMM, better consistency is generated between KCRVs and expected activity values from the response curve of the SIR ionisation chamber convoluted with nuclear decay data.

The first step of the procedure is a preliminary scrutiny of the stated uncertainties, to protect the PMM against data with incomplete uncertainty estimates. For potentially inconsistent data sets, a common uncertainty component is quadratically added to all data to assure that reduced chi squared does not exceed unity. The PMM can smoothly vary between an arithmetic and inverse variance weighted mean, by choosing an appropriate value for the power in the weighting factors. Power moderation is by default implemented in small data sets, since they generally contain insufficient information to generate complete trust in the stated uncertainties. This extra protection against overly optimistic data gives the PMM an edge in robustness. It outperforms other methods, including the most popular method (D-L) used for meta-analysis in clinical trials, as demonstrated in Figure 2 [21].

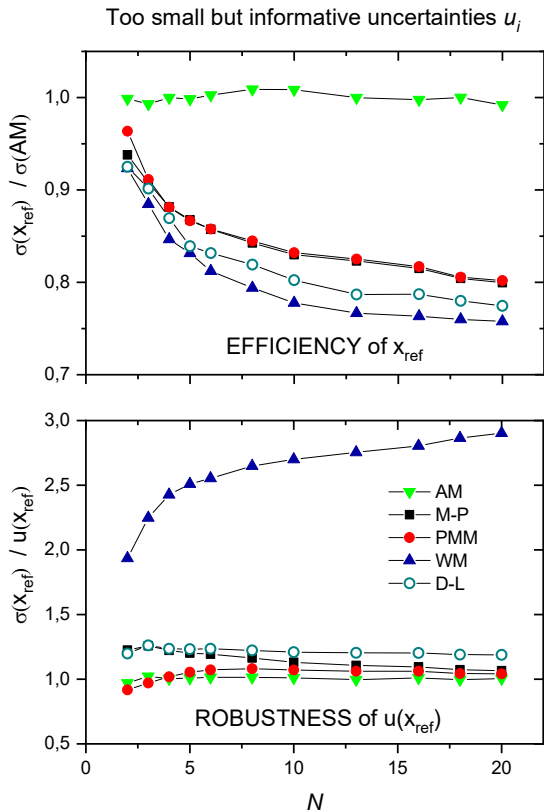


Figure 2: Simulation results for measures of efficiency and robustness of the arithmetic (AM), Mandel-Paule (M-P), power-moderated (PMM), inverse-variance weighted (WM), and Der Simonian-Laird (D-L) mean for discrepant data sets as a function of the number of data. (Top) Standard deviation of the mean around the true value used in the simulation. (Bottom) Ratio of the standard deviation of the mean to the calculated uncertainty. The PMM is almost as robust as the AM, yet more efficient. WM, M-P and D-L underestimate the uncertainty.

## 2.5 Meta-analysis of equivalence

Since mutual confidence in measurements is acquired through equivalence, metrology can inspire trust only if the measurement techniques are under statistical control. This means that each significant source of uncertainty should be identified and appropriately quantified. Trustworthiness is built on the completeness of the uncertainty budget, and conversely it is affected by understatement of uncertainty due to ignorance or desire to impress the world with bold claims of unmatched accuracy. The maturity of a metrological community can be assessed through meta-analysis of interlaboratory comparisons. A graphic tool, the PomPlot [25,26], was developed to visualise equivalence in relation to the stated uncertainties. PomPlots can be made of a single intercomparison, a set of comparisons for a single laboratory, or an overview of comparisons within a specific community [25]. Laboratories can evaluate the quality of their uncertainty estimates through an aggregated PomPlot of their proficiency results [25,26].

Figure 3 shows a combined PomPlot of SIR submissions of activity standards for various radionuclides from member NMIs. The PomPlot displays deviations  $D$  of individual results from the reference value on the horizontal axis and uncertainties  $u$  on the vertical axis, originally using the median absolute deviation (MAD) of each KC data set as the yardstick. A better alternative to the MAD is the characteristic spread parameter  $S$

calculated in the PMM [21], to protect against fortuitously small MAD values in overly consistent data sets. The diagonal lines correspond to a  $z$ -score of  $\pm 1$ ,  $\pm 2$ , and  $\pm 3$ , respectively. The diagonals can be made to represent the  $\zeta$ -score when the  $u$  values are corrected for the uncertainty of the reference value and mutual correlation [21], otherwise the  $\zeta$ -score lines diverge at the top [27]. If all data are normally distributed, the majority is found back within the  $\zeta=\pm 1$  and  $\zeta=\pm 2$  areas, and practically no outlier is found outside the  $\zeta=\pm 3$  area.

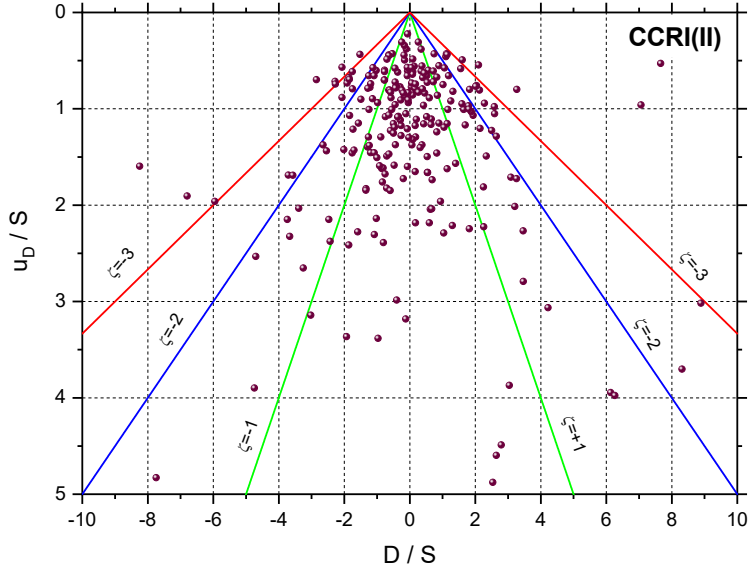


*Figure 3: A combinatorial PomPlot of a non-exhaustive set of key comparison results for activity standardisations of radionuclides, through the SIR (K1) and direct comparisons (K2). Several inconsistent data are due to the difficult standardisation of  $^{125}\text{I}$ . Overall, the uncertainties in the last two decades have been somewhat more homogenous and realistic than in the past (see Fig. 4 in [25] for comparison).*

In Figure 3, there is a small fraction of outliers and data with understated uncertainties which belong at a lower position in the graph. Fortunately, the stated uncertainties turn out to be informative, since they correlate strongly with the deviations from the reference. However, a more linear proportionality was found with the square root of the uncertainty [4,25]. In other words, some uncertainties are overstated and others are understated, even at the highest level of metrology. This observation supports the use of a moderated power in the statistical weights of the PMM. PomPlots of proficiency tests of European radioactivity monitoring laboratories reveal a higher percentage of outliers and a subset with grossly understated uncertainties. It is not uncommon to find a high concentration of trustworthy laboratories near a  $u/S$ -value of 1, since they have a grasp of the typical uncertainties associated with their methods [26,28,29].

### **3 Primary standardisation at the JRC**

#### **3.1 Joint Research Centre**

The Euratom treaty [30] signed in 1957 founded the Joint Nuclear Research Centre (JNRC) of the European Commission (EC) that harbours “a bureau of standards specialising in nuclear measurements for isotope analysis and absolute measurements of radiation and neutron absorption” at the Geel site in Belgium. Euratom’s mission was to contribute to the formation and development of Europe’s nuclear industries, to ensure regular and equitable supply of nuclear materials for peaceful civil uses to the Member States, preventing nuclear materials from being diverted to military use, and guaranteeing high safety standards for the public. In the 1970s, the ‘N’ in JNRC was dropped when the JRC addressed also non-nuclear issues and evolved into the EC’s science and knowledge service.

The Radionuclide Metrology team of the JRC started its pioneering work in 1959 “to ensure that a uniform nuclear terminology and a standard system of measurements are established” (Article 8) [30]. The group developed and applied accurate primary standardisation techniques for radioactivity, measured and evaluated nuclear decay schemes and atomic data. With time, the work was extended to characterisation of nuclear reference materials, the organisation of intercomparisons among European radioactivity monitoring laboratories, and performance of ultra-sensitive gamma-ray spectrometry in an underground facility. Through education and training programs, organisation of workshops and conferences, and scientific publications, nuclear research is promoted and sound methodology is passed on to the metrological community. Particular attention is paid to rigorous uncertainty estimation and data analysis techniques.

Below, an overview of measurement techniques applied at the JRC for primary standardisation work in the last two decades is presented. The methods can be classified into three categories: high-efficiency  $4\pi$  counting, coincidence counting, and counting at a defined solid angle.

#### **3.2 Source preparation**

Two aspects in the preparation of quantitative sources for activity standardisation are usually of crucial importance: achieving an accurate quantification of the amount of radioactive solution contained in the source and a high transparency of the source for the emitted radiation [5,31,32,33,34]. The most accurate quantification is done by mass weighing using the “pycnometer method” with a microbalance calibrated with SI-traceable reference weights, either using the direct method or the substitution method [5,34]. A sufficient amount of solution should be dispensed on a series of sources to reduce the non-negligible random and systematic weighing errors. The radioactive drops are dispensed on an appropriate substrate bespoke to the method used, e.g. on an ultra-thin polymer foil or directly into a scintillator cocktail. Polyvinylchloride-polyvinylacetate copolymer (VYNS) support and cover foils are produced in a controlled manner on a spinning soaped glass plate, and covered with a vacuum evaporated gold layer if conductivity is required (Fig. 4). The source homogeneity is improved by adding seeding and wetting agents [5,33]. The JRC source drier speeds up the drying process significantly by blowing heated nitrogen jets into the drop to curtail the formation of big crystals [31,32]. To avoid contamination with dust particles, the source preparation is performed in a laminar flow of filtered air and the sources are kept dry in dust-free desiccators. Qualitative sources for high-resolution spectrometry can be produced by non-quantitative methods, such as e.g. electrodeposition [35,36,37], vacuum evaporation [32,38], and collection of recoil atoms following alpha decay [39,40].



*Figure 4: Fishing of a gold-evaporated VYNS foil on a large support ring, after it was soaked off a glass plate in the water bath. Upon drying, the wrinkles in the foil straighten out.*

### 3.3 Large Pressurised Proportional Counter

JRC's Large Pressurised Proportional Counter (LPPC) consists of a cylindrical gas chamber and a central planar cathode dividing it into two D-shaped counters with a 21- $\mu\text{m}$ -thick stainless steel anode wire each [41]. A simplified scheme has been published elsewhere [41] and a technical drawing is presented in Figure 5. The LPPC is operated with P10 counting gas, consisting of 90% argon and 10% methane. The counter gas is continuously refreshed, while kept at a constant pressure between 0.1-2 MPa [42]. The LPPC is used as a  $4\pi$  geometry counter aiming at 100% counting efficiency for the activity of beta and alpha emitters, such as  $^{204}\text{Tl}$  [43],  $^{39}\text{Ar}$  [36],  $^{238}\text{Pu}$  [44], and  $^{241}\text{Am}$  [45,46]. Mono-energetic x rays from  $^{55}\text{Fe}$  are used for calibration of the energy threshold. The source deposited on a gold-evaporated VYNS foil is integrated into the cathode. An estimated amount of 0.5% of the alpha particles get absorbed in the foil and remain undetected. The loss of beta particles, which have a continuous energy spectrum, is estimated by varying some conditions, such as the source mass, number of cover foils, and energy threshold. In the particular case of  $^{204}\text{Tl}$ , which has a low-energy beta emission spectrum, the self-absorption varied substantially with carrier concentration [43].

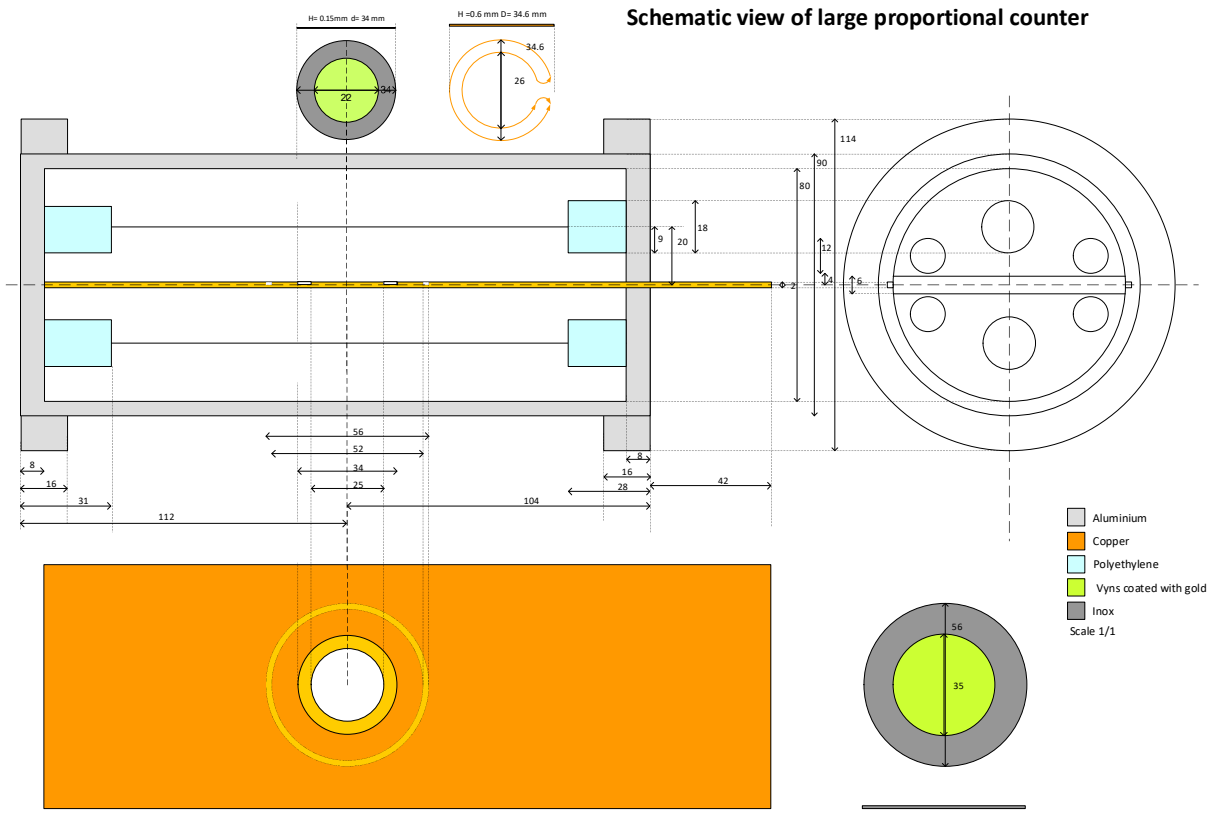


*Figure 5: Design of JRC's large pressurised proportional counter (LPPC). There is a choice of cathodes with a cut-out of 35 mm or 56 mm diameter to accommodate standard (34 mm) or large (55 mm) source substrates, respectively. The source support is a metal ring covered with a gold-coated VYNS foil; a clamp keeps it firmly in position.*

### 3.4 $4\pi \beta\text{-}\gamma$ coincidence counter

The coincidence method [47,48,49,50] offers an alternative to high-efficiency methods for radionuclides which emit at least two distinguishable types of radiation in their decay process, most commonly  $\beta$  or  $\alpha$  particles (or low-energy x rays and Auger electrons from electron capture) followed by  $\gamma$ -ray emissions. The detection set-up consists of two detectors which, ideally, are exclusively sensitive to one type of radiation: a small version of the pressurised gas proportional counter (SPPC) as the particle detector and a 15 cm $\times$ 15 cm NaI(Tl) well-type scintillation crystal as the photon detector. Either by classical electronics [48] or by digital data acquisition [49], the individual count rates in both detectors as well as their coincidence count rate are recorded (Fig. 6). Ideally, the unknown source activity and detection efficiencies can be derived from a single measurement. In practice, the activity is mostly obtained from a linear extrapolation of a series of measurements performed at varying counting inefficiencies approaching zero.



*Figure 6: Dr. Stefaan Pommé and visiting scientist Dr. Hasan Dikmen inspecting the classical electronics used for coincidence counting.*

A photo of the set-up has been published [45] and technical drawings of the SPPC and well NaI crystal are shown in Figures 7 and 8, respectively. The source is placed in the cathode of the SPPC, and the SPPC is then slid inside the 50 mm diameter well of the NaI detector. This ensures a favourable geometry and high detection efficiency for both detectors, thus reducing the time needed for reaching statistical accuracy in the coincidence channel. In the last two decades, coincidence methods have been used to standardise  $^{152}\text{Eu}$  [51],  $^{65}\text{Zn}$  [52],  $^{54}\text{Mn}$  [53],  $^{192}\text{Ir}$  [54],  $^{241}\text{Am}$  [45],  $^{134,137}\text{Cs}$  [55,56],  $^{125}\text{I}$  [57,58], and  $^{124}\text{Sb}$  [59] with accuracies of typically 0.1%–0.5%. For certain radionuclides ( $^{152}\text{Eu}$ ,  $^{192}\text{Ir}$ ,  $^{241}\text{Am}$ ), the efficiencies were high enough to use a sum-counting method to obtain the decay rate directly from the sum of the detector count rates minus the coincidence count rate.

Formerly, the JRC operated an old coincidence set-up with an atmospheric pill-box gas counter, sandwiched between a bottom and top 7.6 cm×5.1 cm cylindrical NaI crystal inside a lead castle. The set-up without the gas counter was used as a photon-photon coincidence counter for the standardisation of  $^{125}\text{I}$  [57], in which the efficiency was varied by source covering. The same x-x,y coincidence technique was applied with two moveable integral line NaI detectors at various distances from the source. Both approaches yield the correct result in a single measurement under any condition, without the need for extrapolation [57].

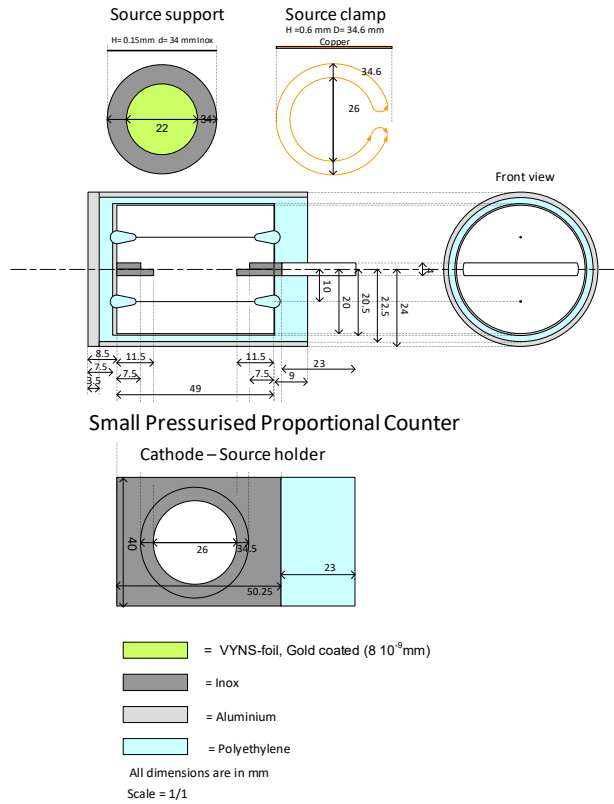


*Figure 7: Technical drawing of the small pressurised proportional counter (SPPC), showing the dimensions of the source support, the cathode acting as source holder, and the gas counter with two anode wires.*

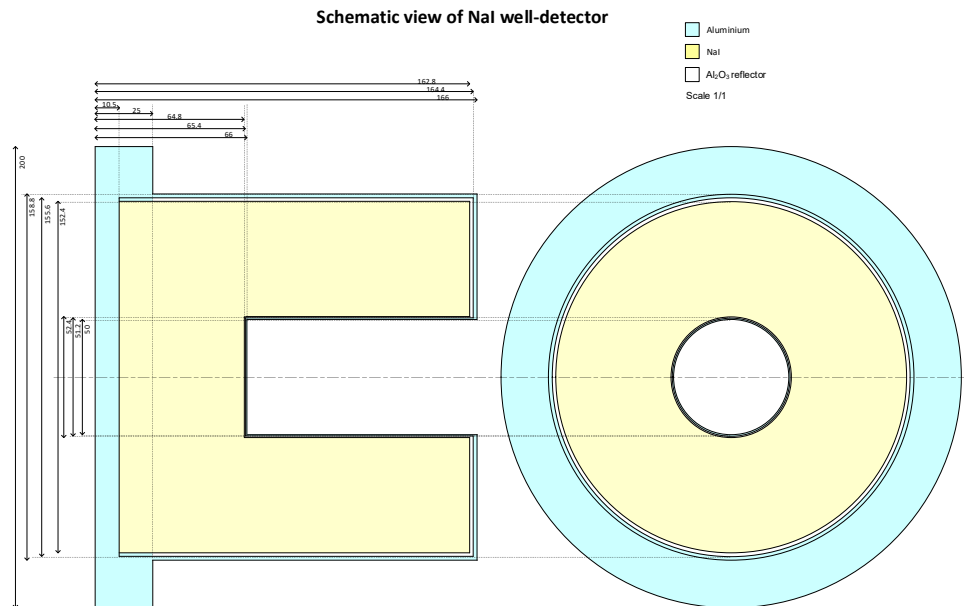


*Figure 8: Drawing of the NaI(Tl) well detector used in the  $4\pi\beta\text{-}\gamma$  coincidence (and sum) counting method, when it hosts the SPPC in the well. It is also used standalone for  $4\pi\gamma$  counting.*

### 3.5 $4\pi\gamma$ counter

High-efficiency photon detection systems are ideally suited for  $4\pi\gamma$  counting, which is an advantageous standardisation technique for radionuclides emitting cascades of  $\gamma$  rays after decay [2,60]. The JRC uses the well-type NaI(Tl) detector in Figure 8, as well as an advanced version with a larger (20.3 cm $\times$ 20.3 cm) NaI(Tl) crystal and a narrow (2.5 cm) and deep (13.4 cm) well, as shown in Figure 9. As the number of coincident photons per decay increases, the probability of non-detection and its associated uncertainty approach zero. The radionuclide-specific total counting efficiency can be determined by Monte Carlo simulation of the photon-particle transport or by bespoke analytical models [61,62,63,64]. The success of the modelling depends primordially on the accuracy of the input parameters, such as chemical composition and dimensions of the materials, as well as attenuation coefficients, particle ranges, and bremsstrahlung production data.

The activity of  $^{152}\text{Eu}$  [51],  $^{192}\text{Ir}$  [54],  $^{166m}\text{Ho}$  [65] could be standardised by  $4\pi\gamma$  counting with close to 100% counting efficiency, owing to their complex decay scheme, whereas this was not the case with  $^{124}\text{Sb}$  [59]. Reference activity values for PET nuclides (e.g.  $^{18}\text{F}$ ,  $^{111}\text{In}$ ) were determined for proficiency tests of hospital calibrators [10,11]. The large detector and its portable lead shield can in principle be moved to production centres of short-lived PET nuclides for in-situ standardisations. Even though single  $\gamma$ -ray emitters are not ideally suited for the  $4\pi\gamma$  counting method, the thermal neutron flux in a research reactor was determined with 1.5% accuracy through a measurement of the  $^{198}\text{Au}$  activity in an irradiated gold monitor [66]. The same instrument was used for the photon sum-peak counting method for the standardisation of  $^{125}\text{I}$ , in which the detection efficiency is determined from the ratio between the single photon detections and coincidence peaks [57] and correcting properly for random coincidences [58]. Both standardisation methods apply to point sources, but can be expanded to voluminous sources if heterogeneity of the detection efficiency is taken into account.

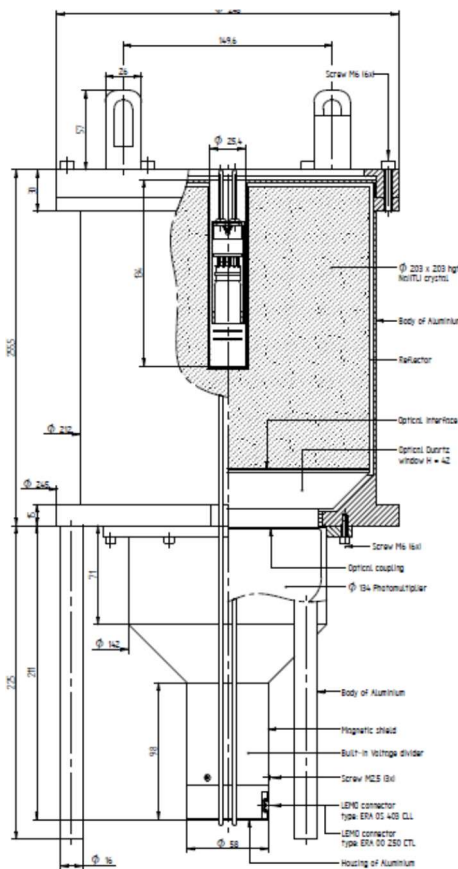


*Figure 9: Technical drawing of the NaI(Tl) well detector specifically designed for the  $4\pi\gamma$  counting method. It can also be used for  $4\pi\beta\text{-}\gamma$  coincidence counting when inserting plastic scintillators and a slender photomultiplier tube into the well.*

### 3.6 CsI(Tl) sandwich spectrometer

The windowless  $4\pi$  CsI(Tl) sandwich spectrometer [67] consists of two cylindrical CsI(Tl) scintillation crystals with a semispherical cavity in their front faces. Pictures have been published [45] and a technical drawing is shown in Figure 10. The radioactive source is pressed between both crystals and emits its radiation quasi perpendicularly towards the inner wall of the spherical cavity formed in the centre of the detector. Radiation-induced scintillations are detected by photomultiplier tubes at the back of the crystals. The gains of both signals are matched to obtain symmetrical sum peaks proportional to the energy deposited by the 59 keV  $\gamma$ -ray of a  $^{241}\text{Am}$  check source. The set-up is mounted inside a source-interlock chamber, which is continuously flushed with dry hydrogen to protect the hygroscopic CsI(Tl) crystals from contact with humidity in the air.

The detector is sensitive to alpha and beta particles, as well as x rays and gamma rays. It is limited at the low-energy side – up to about 10 keV – due to electronic noise and at the high-energy side – above a few hundreds of keV – due to partial transparency to photons. The instrument is unique among standardisation laboratories, yet it has an unparalleled quality to detect the decay of radionuclides with complex decay schemes at quasi zero detection inefficiency. This was demonstrated in key comparisons of  $^{152}\text{Eu}$  [51],  $^{238}\text{Pu}$  [44],  $^{192}\text{Ir}$  [54],  $^{124}\text{Sb}$  [59], and  $^{166m}\text{Ho}$  [65]. The wall of the internal cavity can be covered with plastic caps to stop the particles from being detected, thus allowing to switch from the  $4\pi$  mixed particle-photon counting method to  $4\pi$  photon counting. The activity of  $^{125}\text{I}$  has been standardised with both options, each requiring particular detection efficiency formulas [57,58].

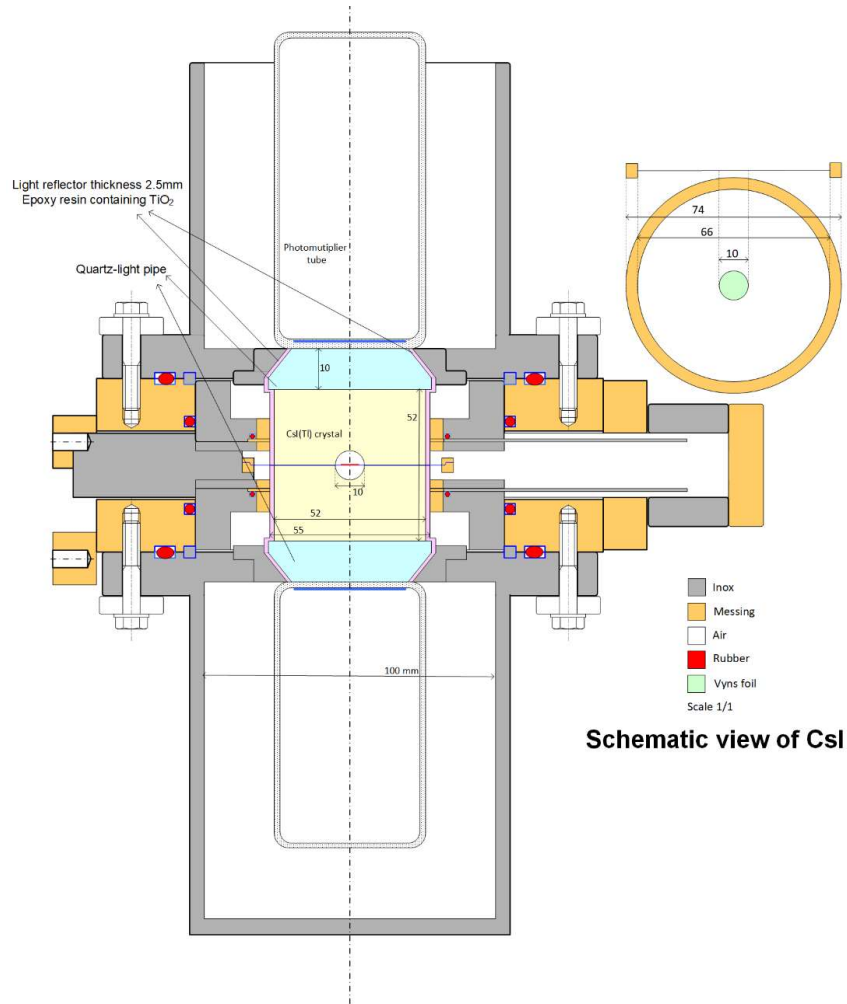


Figure 10: Drawing of the CsI(Tl) sandwich spectrometer and the source-interlock chamber. The source support (top right) is a VYNS foil covering a 10-mm-diameter hole in a 3.2- $\mu\text{m}$ -thick mylar foil pressed between solid brass rings.

### 3.7 Counting at a defined solid angle

High-efficiency counting of  $\alpha$  emitters in a solid source has the disadvantage that the  $\alpha$  particles emitted at the smallest angles to the source plane can get absorbed in the carrier foil without being detected. Therefore, metrological accuracy can be gained by counting only the particles emitted perpendicularly to the source plane within a well-defined small solid angle (DSA) and multiplying the count rate with the geometry correction factor [68]. The JRC has two  $\alpha$ -DSA counting set-ups consisting of a source chamber, distance tube, and a circular diaphragm in front of a large PIPS detector. Pictures and a technical drawing have been published [32]. Variations in geometrical efficiency can be realised by replacing diaphragms and distance tubes.

Accurate measurements of the distance between source and diaphragm as well as the diaphragm radius were performed by optical techniques [32,69] (Fig. 11), which have recently been automated with a 3D-coordinate measuring machine [70]. The solid angle subtended by the detector can be addressed with exact mathematical algorithms for circular and elliptical configurations [71,72,73,74], however the method gains significant robustness by taking into account the source activity distribution obtained with digital autoradiography [69,75,76]. An accuracy of 0.1% can be achieved on the activity. The solid angle is quite insensitive to temperature changes, provided that the diaphragm and distance tube have equal thermal expansion coefficients. The technique has been successfully applied to activity standardisation of  $^{238}\text{Pu}$  [44],  $^{241}\text{Am}$  [45], and  $^{231}\text{Pa}$  [27], certification of reference materials with tracer activity [77], and half-life measurements of  $^{233}\text{U}$  [78],  $^{243}\text{Am}$  [79],  $^{225}\text{Ac}$  [40,80],  $^{230}\text{U}$  [81], and  $^{235,238}\text{U}$ .



*Figure 11: Dr Maria Marouli optically measuring the thickness of a source using a vertically traveling microscope with distance probe, which is currently replaced by a 3D-coordinate measuring machine [70].*

The DSA counting technique is not suitable for  $\beta$  emitters due to the high probability of scattering processes. However, two different set-ups have been constructed for activity measurements of x-ray emitters. Both have a source chamber, distance tube with diaphragm, and gas proportional counter with front window. In one counter, the window foil is sufficiently strong and thick to allow for vacuum pumping in the source chamber. A drawing of the set-up is shown in Figure 12. It has been used for an activity standardisaton [82] and half-life measurement [83] of  $^{55}\text{Fe}$ . The other set-up has an ultra-thin window to minimise photon absorption, however it requires the use of helium gas in the source chamber to counterbalance the gas pressure in the detector. In the past, it was used to make a set of x ray fluorescence sources for the calibration of Si(Li) detectors [84,85].

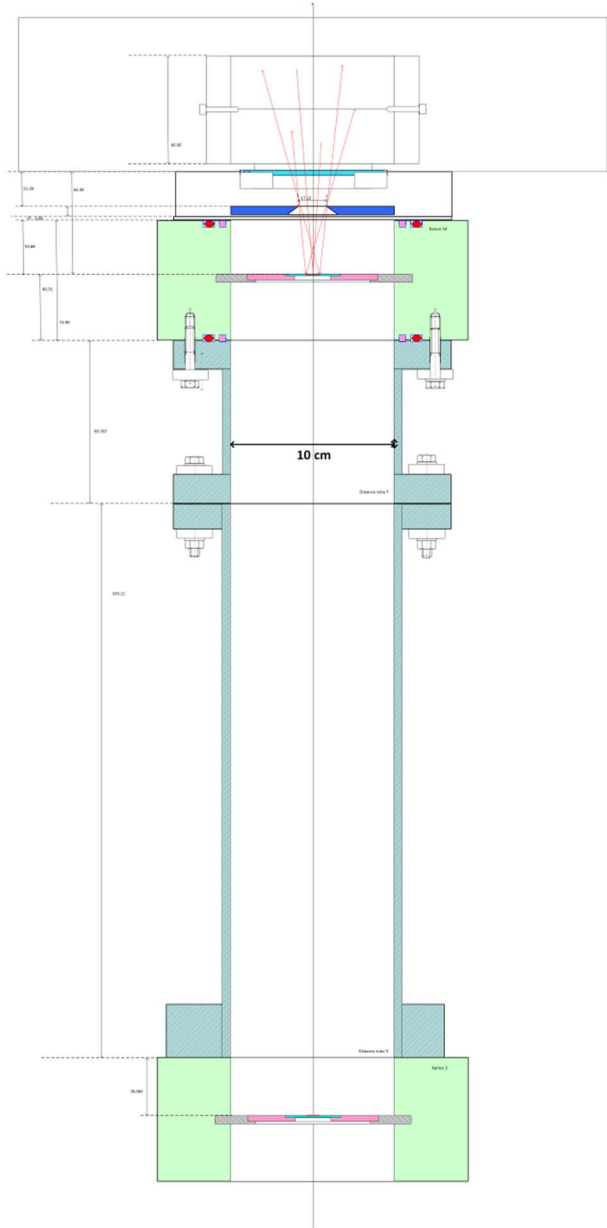


*Figure 12: Drawing of one of the x ray DSA counters consisting of two source chambers separated by a distance tube, a diaphragm, and a gas proportional counter with a 25- $\mu\text{m}$ -thick beryllium entrance window.*

### 3.8 Liquid Scintillation Counters

Through the work of Dr. T. Altzitzoglou, the JRC performed liquid scintillation counting (LSC) with the CIEMAT/NIST (C/N) efficiency tracing technique, as well as the triple-to-double-coincidence ratio (TDCR) method [86,87]. The C/N  $4\pi$  liquid scintillation measurements were performed using a Packard Tri-Carb model 3100 TR/AB (PerkinElmer, Inc., Waltham, MA, USA) and two Wallac Quantulus 1220 (PerkinElmer, Inc.) liquid scintillation spectrometers (Fig. 13). All instruments were operated with two phototubes in sum-coincidence mode at a temperature of about  $12^\circ\text{C}$ . The TDCR set-up was developed and constructed at the JRC. It consisted of three photomultipliers surrounding the liquid scintillator vial at  $120^\circ$ , the signals of which were used to form double and triple coincidences.

Both methods require rather complex calculation techniques to derive the counting efficiency of the nuclide under study. This is done using the free parameter model, describing the physicochemical processes and statistics involved in photon emission. The free parameter can be deduced from the measurement of a tracer

(C/N) or from the coincidence ratio (TDCR). LSC was applied for the standardisation of a suite of reference materials and solutions for key comparisons, measurements of decay data and characterisation of materials for proficiency testing exercises (e.g. [88]). Examples of nuclides measured are  $^3\text{H}$  (as tritiated water),  $^{90}\text{Sr}$ ,  $^{124}\text{Sb}$ ,  $^{125}\text{I}$ ,  $^{151}\text{Sm}$ ,  $^{152}\text{Eu}$ ,  $^{166\text{m}}\text{Ho}$ ,  $^{177}\text{Lu}$ ,  $^{204}\text{Tl}$ ,  $^{238}\text{Pu}$ , and  $^{241}\text{Am}$ .

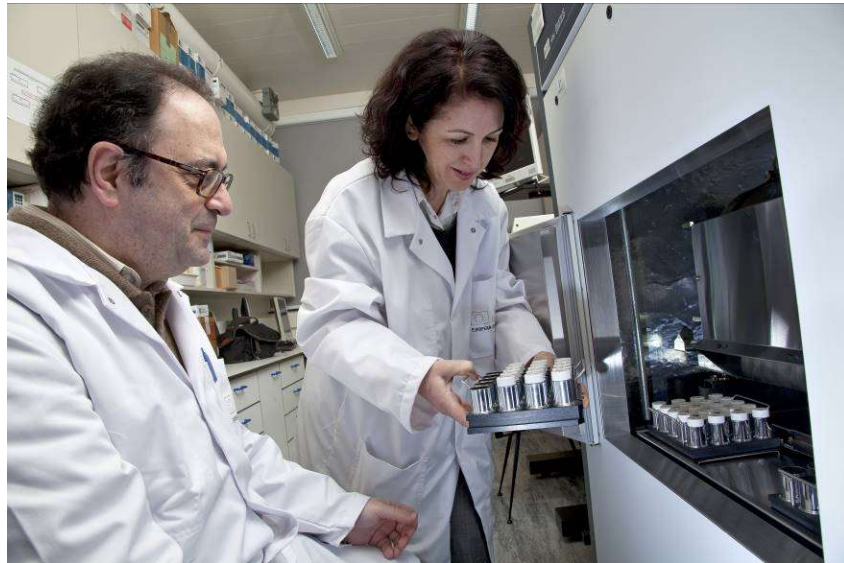


*Figure 13: Dr. Timotheos Altzitzoglou and visiting scientist Dr. Gülsen Ozcyn operating an ultra-low background liquid scintillation spectrometer.*

### 3.9 PomPlot of key comparisons

Figure 14 shows PomPlots [25,26] of the key comparisons of activity measurements to which the JRC participated in the last two decades. The reference value was calculated from the PMM [21] of the official results from the NMIs, with exclusion of values based on secondary standardisation techniques and extreme values identified on statistical grounds [21]. The x-axis shows the difference between the measurement results and the reference value, and the y-axis the corresponding uncertainty value including the uncertainty of the reference value and a correction for correlation. Therefore, fixed  $\zeta$ -scores lines appear linear in the PomPlot. For most KCs, the data sets are rather consistent and few outliers are identified. Only in the case of  $^{125}\text{I}$ , a scientifically motivated selection of unbiased data was made instead of a consensus value of the majority of the data. This is due to a bias towards low values caused by volatility of iodine, incomplete modelling of the deexcitation process in LSC techniques, and inadequate corrections for accidental coincidences [58] in the photon sum-peak counting method [57].

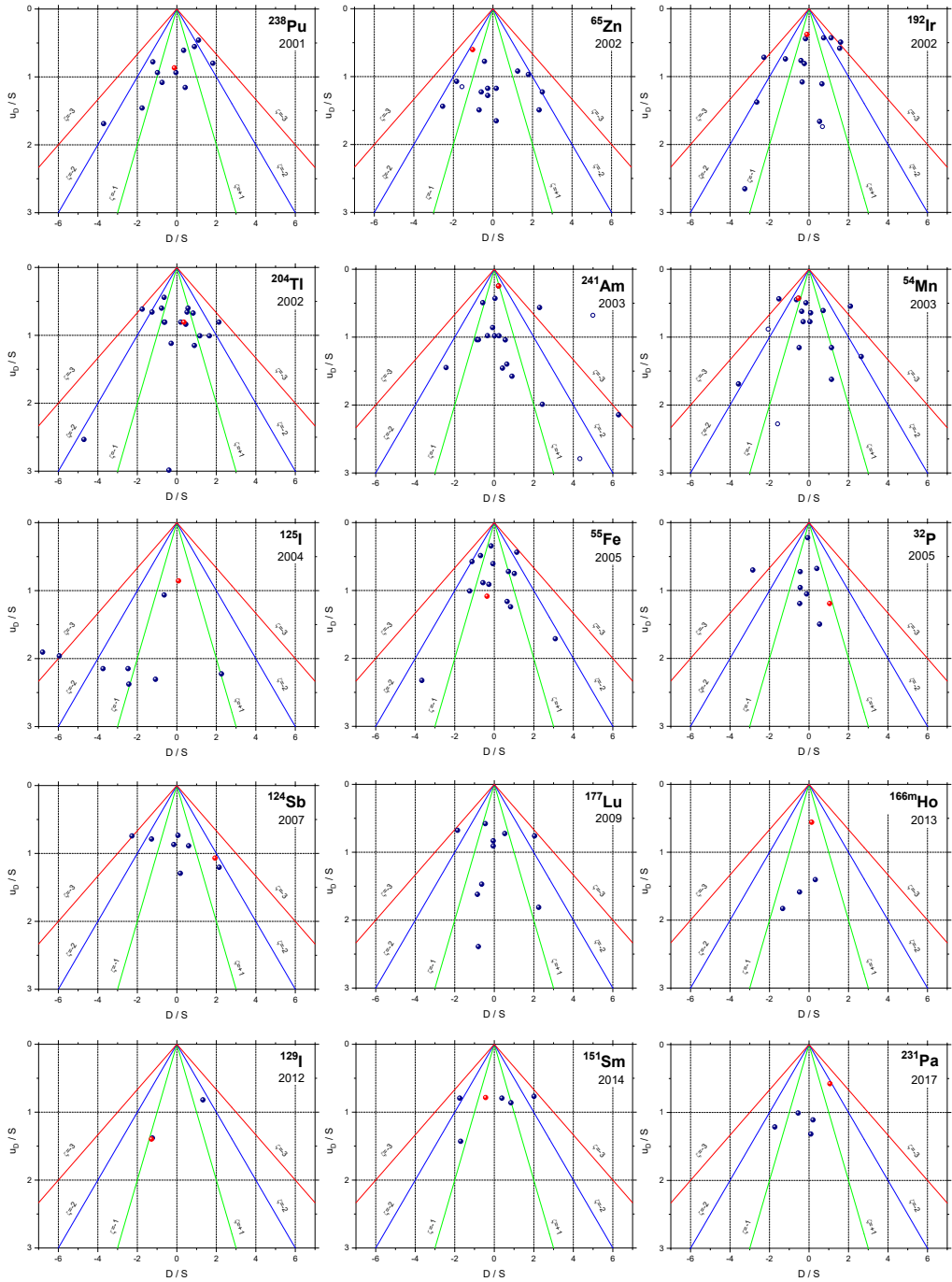


**Figure 14:** PomPlots of CCRI(II) K2 key comparisons of activity. The radionuclides and the year of execution are indicated in the corner of the graphs. The red dots represent the JRC results. In the case of  $^{177}\text{Lu}$  [89,90], the JRC result at  $u/\text{S}=4.5$  and  $\zeta=0.6$  is off the scale due to the large uncertainty estimate. The same applies to extremely discrepant or uncertain data from other NMIs.

A signature PomPlot of JRC's results is presented in Figure 15, which aggregates all the red dots from Figure 14. It is immediately apparent that most of the JRC results are near the top of the graph, which means that their stated uncertainties are lower than state-of-the-art in the field. More importantly, the JRC data are very reliable, since 80% of the results score within  $\zeta=\pm 1$  and all of them are within  $\zeta=\pm 2$ . This exceptional track record is based on redundancy of methods and realistic assessment of measurement uncertainty. The

JRC is famous for using a multitude of techniques to underpin the final result, e.g. 7 methods for  $^{125}\text{I}$ , 6 for  $^{241}\text{Am}$ , 5 for  $^{192}\text{Ir}$  and  $^{166\text{m}}\text{Ho}$ , and 4 for  $^{238}\text{Pu}$ . These methods are mutually consistent at a high level of accuracy, as demonstrated in Figure 16 by the aggregate PomPlot of the partial results obtained with the individual techniques.

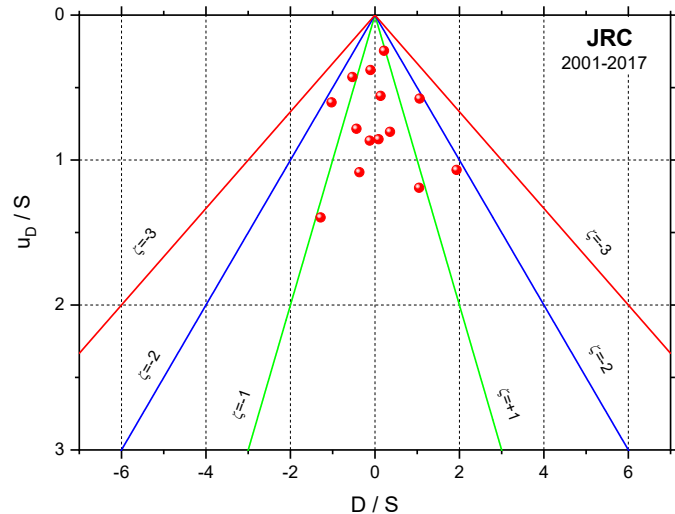


Figure 15: Aggregate PomPlot of JRC's results in the KCs depicted in Figure 14. The distribution of the data shows that the measurements are very accurate and the stated uncertainties are reliable.

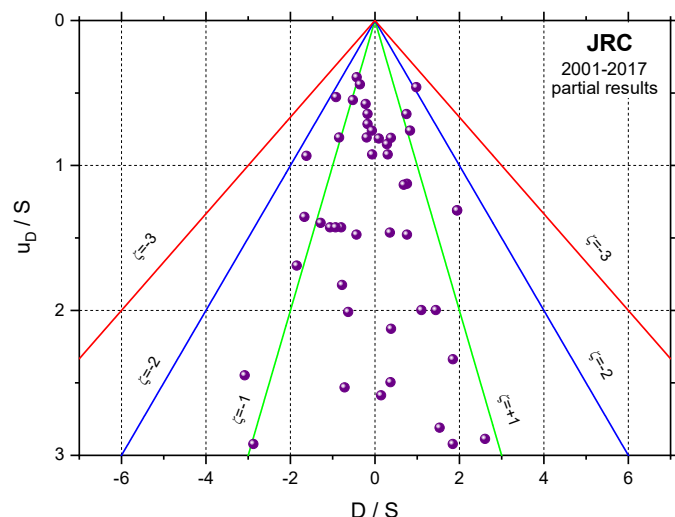


Figure 16: Aggregate PomPlot of JRC's partial results with individual primary standardisation techniques. The results are mutually consistent and free of bias.

Achieving a full uncertainty budget with ambitious but realistic claims on precision and accuracy constitutes one of the most challenging aspects of metrology. Redundancy of methods has often proved to be indispensable to explore the strengths and weaknesses of specific approaches and to gain confidence in the accuracy and precision attributed to the eventual activity reference value.

### 3.10 Secondary standardisation

Secondary standardisations are performed using primary-calibrated re-entrant pressurised ionisation chambers (IC) in combination with a current-measuring device or a charge capacitor with voltage over time readout. Thus, activity reference values are provided for proficiency tests of European monitoring laboratories [88] and nuclear calibrators in hospitals [10,11].

Whereas the linearity range of nuclear counting devices is hampered by pulse pileup and dead-time effects [3], ICs can boast a wide dynamic range over which the ionisation current varies proportionally with the measured activity [91]. Owing to their favourable stability, reproducibility, and linearity properties, ICs are well suited for the measurement of the half-life of gamma-emitting radionuclides over periods varying from hours to decades.



*Figure 17: Top view of the ionisation chamber IC1 of the JRC (top) and front view of the IC1 in a lead brick shielding at the right, its electronics, and below the charge-integrating air capacitor in a lead shield (bottom).*

## 4 Nuclear decay data

### 4.1 Need for reliable decay data

Quantitative analyses and SI-traceable measurements of radioactivity through particle and photon detection crucially rely on the accuracy of the associated emission probabilities in the decay of the particular radionuclide. Other critical nuclear data are half-lives, branching ratios, emission energies, total decay energies, and cross sections for nuclear reactions. Over the years, the scientific community has measured, compiled and evaluated decay data and combined them with theoretical studies with the aim of deriving consistent nuclear decay schemes with realistic uncertainty budgets [92,93]. These reference data are highly desired input for modelling codes in numerous applications and for theoretical understanding of the structure of the nucleus.

### 4.2 Intermediate half-life measurements

Through the exponential-decay law the activity of a radionuclide in a sample can be extrapolated to an arbitrary point in the future or the past [94,95]. The validity of these extrapolations in time depends critically on the accuracy of the half-life value and the reliability of its assigned uncertainty. Nuclear half-life determinations through repeated decay rate measurements in stable measurement conditions have long been perceived as easy experiments with straightforward data analysis. In the 20th century, it was common practice to publish half-life experiments in a casual, incomplete reporting style, which concealed the level of attention paid to the stability of the measurement conditions, the integrity of the data analysis, and the completeness of the uncertainty budget. As a consequence of this relaxed attitude, the literature abounds with poorly documented experiments and highly discrepant half-life data, which constitute the somewhat shaky foundation of the recommended data set for the most relevant radionuclides. In the last decades, insight was gained in the propagation of errors and the essential information required for complete reporting [95,96,97,98,99]. Owing to the increased awareness, current papers on half-life measurements from NMIs have become richer in detail and the uncertainty budgets more realistic. With the enhanced rigor in experimental execution and data analysis, the metrological community is currently achieving better consistency at a higher level of accuracy than in the past [99].

A least-squares fit of exponential functions to a measured radioactive decay rate series provides an estimate of the half-life and its statistical uncertainty in the assumption that all deviations from the theoretical curve are purely of a random nature. The corresponding uncertainty propagation towards the half-life value  $T_{1/2}$  decreases proportionally with the square root of the number of measurements [98]. This result may be biased and the error underestimated as soon as the experiment suffers instabilities that exceed the duration of individual measurements [95,96,97,99]. Medium-frequency perturbations may be observable as autocorrelated structures in the residuals from the fit to the decay curve. Typical examples are daily or annual oscillations due to environmental influences, jumps in detection efficiency due to occasional source repositioning, step functions due to instrument scaling switches and recalibrations, and non-random variations in background and impurity activity. An empirical decomposition algorithm has been designed to separate medium-frequency effects from the random statistical component in the fit residuals, such that custom error propagation factors to the half-life can be calculated [99].

Systematic errors, however, lead to a biased fit without leaving a visible trace in the residuals. The associated error propagation does not reduce by performing additional decay rate measurements [95,96,97]. Common examples are under- or overcompensation of count loss through pulse pileup and system dead time, systematic errors in spectral analysis and corrections for interfering nuclides and background signals, source degradation and non-linearities or slow changes in detector response. Taking these aspects properly into account requires a comprehensive understanding of the metrological limitations of the set-up. In gamma-ray spectrometry, the systematic errors can be significantly reduced by co-measuring a long-lived reference nuclide with  $\gamma$ -ray emissions in the same energy region. The strengths and weaknesses of the reference source method were demonstrated for  $^{145}\text{Sm}$  and  $^{171}\text{Tm}$  half-life measurements performed at the Paul Sherrer Institute (PSI) [100,101].

The JRC has published several cases of good practice in half-life measurements using various instruments, i.e. re-entrant ionization chambers [91,102,103,104,105,106], HPGe detectors [80,81,104,105,109], NaI(Tl) scintillation detectors [80,81,104], liquid scintillation counters [81,106], the CsI(Tl) sandwich spectrometer [80,81], planar ion-implanted silicon detectors [39,80,81,107,108,110], x ray [83] and alpha-particle defined solid angle counters [80,81], and a pressurized proportional counter [41,80,81]. Over a period of 3 decades,

the JRC was the only institute that published two unbiased values for the half-life of  $^{109}\text{Cd}$  [97,105], whereas other data in the literature were discrepant (Fig. 18). This was recently confirmed through new measurement results from the NIST and the NPL [111]. A similar discrepancy between the literature values of the  $^{55}\text{Fe}$  half-life was solved with the most stable data set collected over a period of 18 years [41,97], consistent with a previous measurement at the JRC [83] and a recent result from the PTB [112] (Fig. 19). Extensive research was done on important nuclides for detector calibration ( $^{54}\text{Mn}$ ,  $^{65}\text{Zn}$ ,  $^{109}\text{Cd}$ ,  $^{22}\text{Na}$ ,  $^{134}\text{Cs}$ ), medically interesting isotopes ( $^{177}\text{Lu}$ ,  $^{171}\text{Tm}$ ,  $^{99\text{m}}\text{Tc}$ ), and in particular alpha-emitters considered for alpha immunotherapy, such as the decay products in the  $^{230}\text{U}$  [81,107,113] and  $^{225}\text{Ac}$  series [39,40,80] and  $^{227}\text{Th}$  [109] from the  $^{227}\text{Ac}$  series.

The level of attention paid to every detail in the uncertainty budget is exemplified in an answer to a critique on a paper regarding the  $^{209}\text{Po}$  half-life [110]. The linearity of the nuclear counting methods is well controlled by in-house made live-time modules which impose extending or non-extending dead time on the detection system, and additionally by taking into account secondary cascade effects between pulse pileup and dead time [3]. The linearity of the ionisation chamber is established by integrating the charge over an air capacitor, as demonstrated by achieving the most accurate half-life measurement of the medically important diagnostic nuclide  $^{99\text{m}}\text{Tc}$  over the full working range of the instrument [91]. Its linearity can be further perfected by compensating for a small anti-correlation with ambient humidity [114].

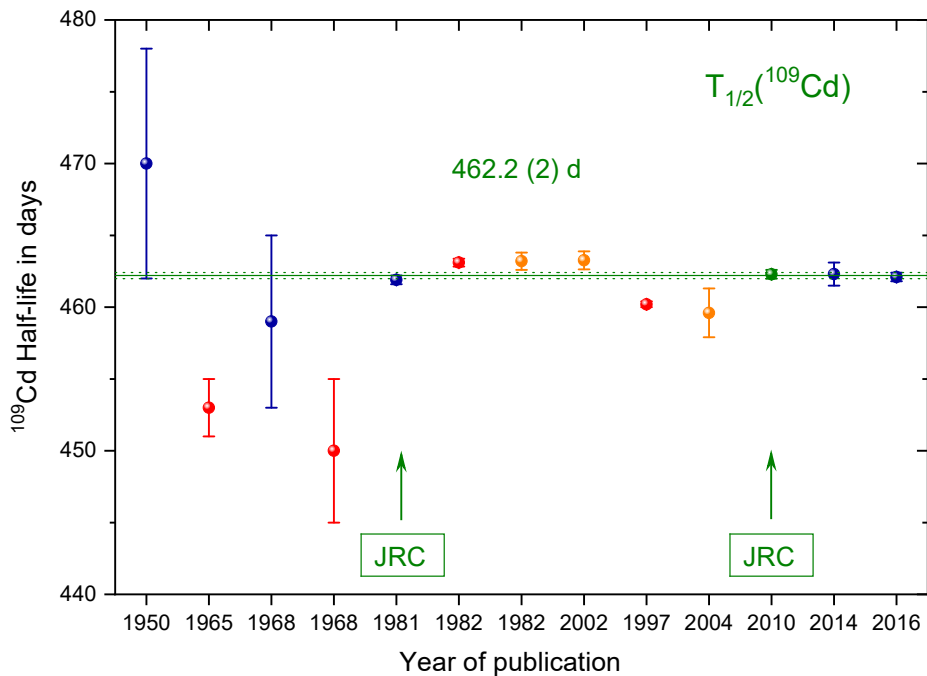


Figure 18: Overview of  $^{109}\text{Cd}$  half-life measurement results, their standard uncertainties, and their year of publication [105,111]. The data of 1981 and 2010 are from the JRC. The line corresponds to a mean of the three most recent values.

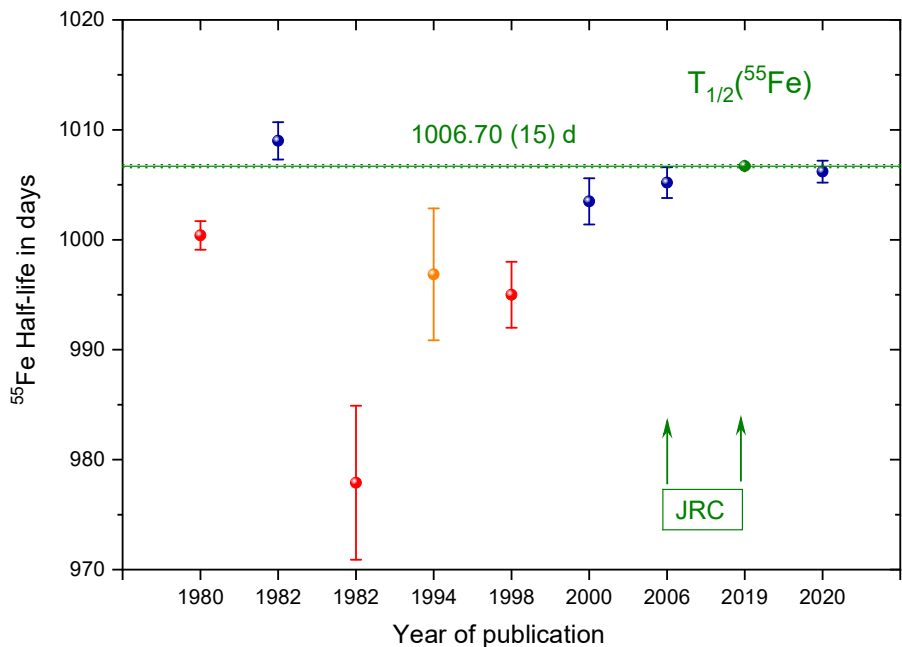
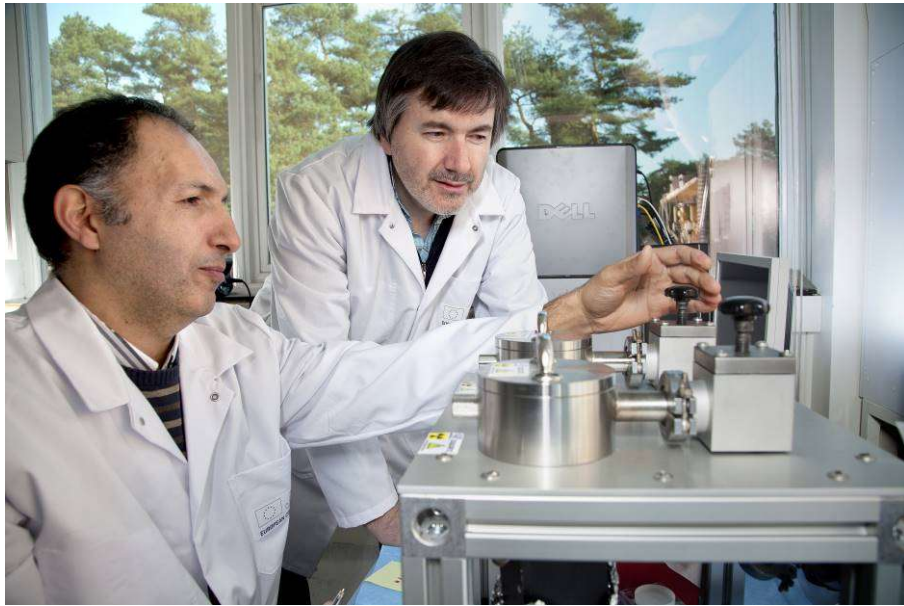


Figure 19: Overview of <sup>55</sup>Fe half-life measurements, their standard uncertainties, and their year of publication [41,112]. The data of 2006 and 2019 are from the JRC and the line corresponds to JRC's most accurate value.

### 4.3 Short and long half-life measurements

Sampling a decay curve is just one method to determine a half-life, applicable only on a ‘human’ time scale. For very short and very long half-lives, say below the second region and above the century region, other techniques are more suitable. Short lifetimes of excited nuclear levels ranging between about 1 ps to several ns are measured by the Recoil Distance Doppler-Shift method in specialised laboratories. Nano- and microsecond nuclear states are mostly measured electronically in delayed coincidence experiments or by time interval analysis. Extremely long half-lives exceeding a century are commonly determined through a specific activity measurement. These techniques and their sources of uncertainty are discussed in a review paper [95], together with propagation factors for applications in spectrometry, nuclear dating, activation analysis, and dosimetry. The fact that it is frequently downloaded underlines the fundamental importance of the exponential-decay law.

The JRC determined the half-life of the short-lived decay products in the <sup>230</sup>U [113] and <sup>225</sup>Ac [40] decay chains by delayed coincidence measurements using digital data acquisition in list mode. The experiments were performed in a small vacuum chamber with an ion-implanted planar silicon detector, measuring alpha and beta particle energies from a weak parent source facing the sensitive area at close distance (Fig. 20). Delayed coincidence spectra were built from the time differences between signals from the energy window of the parent and progeny nuclides, respectively. The true parent-progeny coincidences take an exponential shape, whereas random coincidences show up as a flat component. To avoid the problem of bias in least-square fitting to Poisson-distributed data (instead of normally distributed data), unbiased half-life values were obtained with a maximum likelihood method, a moment analysis, and a modified least-squares fit [115].



*Figure 20: Dr. Stefaan Pommé and visiting scientist Dr. Abdullah Dirican at the small vacuum chambers with planar silicon detectors used for measurements of half-lives in the  $^{230}\text{U}$  and  $^{225}\text{Ac}$  decay series, as well as  $^{209}\text{Po}$ .*

The half-lives of the long-lived nuclides  $^{129}\text{I}$  [116,117],  $^{151}\text{Sm}$  [118,119],  $^{231}\text{Pa}$  [27],  $^{233}\text{U}$  [78],  $^{243}\text{Am}$  [79] were determined through their specific activity, i.e. the activity per quantity of atoms of this particular radionuclide, e.g. expressed in Bq per gram. The specific activity is proportional – via the molar mass and the Avogadro number – to the decay constant, i.e. the ratio between the activity and the number of atoms of a nuclide. The metrology is based on three fields of expertise: mass metrology, mass spectrometry (or coulometry, titration), and absolute activity measurements. The tasks at hand are the careful weighing of the amount of material in solution, the determination of the relative amount of the element and isotope of interest, and the measurement of the massic activity of the specific radionuclide. The attainable accuracy is in the 0.1% region, but can be compromised if the chemical state of the element in solution is not exactly known. The mass content can be determined relative to a reference solution with known amounts of another isotope and by performing isotope dilution mass spectrometry of different mixtures of both solutions.

An alternative route is through analysis of radionuclide mixtures both by mass spectrometry and activity spectrometry. For example, by determining the  $^{243}\text{Am}/^{241}\text{Am}$  activity ratio and isotopic amount ratio in an americium reference material [120] by high-resolution alpha-particle spectrometry and thermal ionisation spectrometry, respectively, the half-life value for  $^{243}\text{Am}$  could be determined relative to  $^{241}\text{Am}$  [79]. In a similar manner, the half-life ratio of  $^{235}\text{U}/^{234}\text{U}$  could be derived from high-resolution alpha-particle spectrometry on three uranium materials enriched in  $^{235}\text{U}$  and containing traces of  $^{234}\text{U}$  [121]. Since the  $^{234}\text{U}/^{238}\text{U}$  half-life ratio of the parent-progeny pair  $^{238}\text{U}-^{234}\text{U}$  is known from mass spectrometric analyses of uranium material in ‘secular equilibrium’, also the half-life ratio of  $^{235}\text{U}/^{238}\text{U}$  could be determined with 0.5% accuracy.

#### 4.4 Alpha-particle emission probabilities

Alpha-particle spectrometry is a radionuclide assay method with a wide range of applications [122,123]. In the user community, measurements are commonly performed with ion-implanted silicon detectors on thin sources, with the aim of determining absolute activities or activity ratios of alpha-emitting nuclides. Strong features of the technique are the low background levels that can be achieved due to low sensitivity to other types of radiation, the intrinsic detection efficiency close to unity which reduces the efficiency calculation to a geometrical problem, and the uniqueness of the energy spectra for each  $\alpha$ -decaying nuclide. The main challenge is the limited energy resolution, even for thin sources with low self-absorption, which causes alpha energy peaks to be partially unresolved due to their width and low-energy tailing. Spectral deconvolution often requires fitting analytical functions to each peak in the alpha spectrum. True coincidence effects

between alpha particles and subsequently emitted conversion electrons can cause distortions of the alpha spectra, which lead to significant changes in the apparent peak area ratios.

The JRC has a set of high-resolution alpha-particle spectrometers dedicated to reference measurements of alpha emission probabilities, in order to improve the nuclear decay scheme of heavy radionuclides [32]. Thin, homogeneous sources are prepared with vacuum evaporation and electrodeposition techniques [5,37,124]. Small planar ion-implanted silicon detectors with  $50\text{ mm}^2$ - $150\text{ mm}^2$  active area are used for optimum energy resolution. The feedback capacitor in the pre-amplifier is adapted to the detector capacitance for noise reduction. The detector flange and the preamplifier housing are temperature stabilised by circulating water from a thermostatic bath. In addition, an off-line mathematical peak stabilisation method [125,126] is applied to reduce peak shift in measurement series to one spectral bin width, even if the campaign extends over years. A strong magnetic field is applied on top of the source to deflect interfering conversion electrons away from the detector [127].

The fluctuations of the energy loss of charged alpha particles by ionisation collisions when travelling through thin layers of matter is represented by the Landau function, which corresponds to the mirror shape of the characteristic peaks in measured alpha-energy spectra. The Landau function consists of a complex integral, which is inconvenient for implementation in peak fitting software. Spectral fitting is done instead with a line shape model 'BEST' based on the convolution of a Gaussian with up to 10 left-handed exponential tailing functions and up to 4 right-handed exponentials [128]. It can deal with a wide range of energy resolutions, even down to the level where the peaks look like step functions [129]. It is the energy resolution and counting statistics of the measured spectra that determines the number of tailing parameters needed to reproduce the peak shape with sufficient accuracy [128]. Common spectra are well reproduced with up to three tailing parameters (Fig. 21).

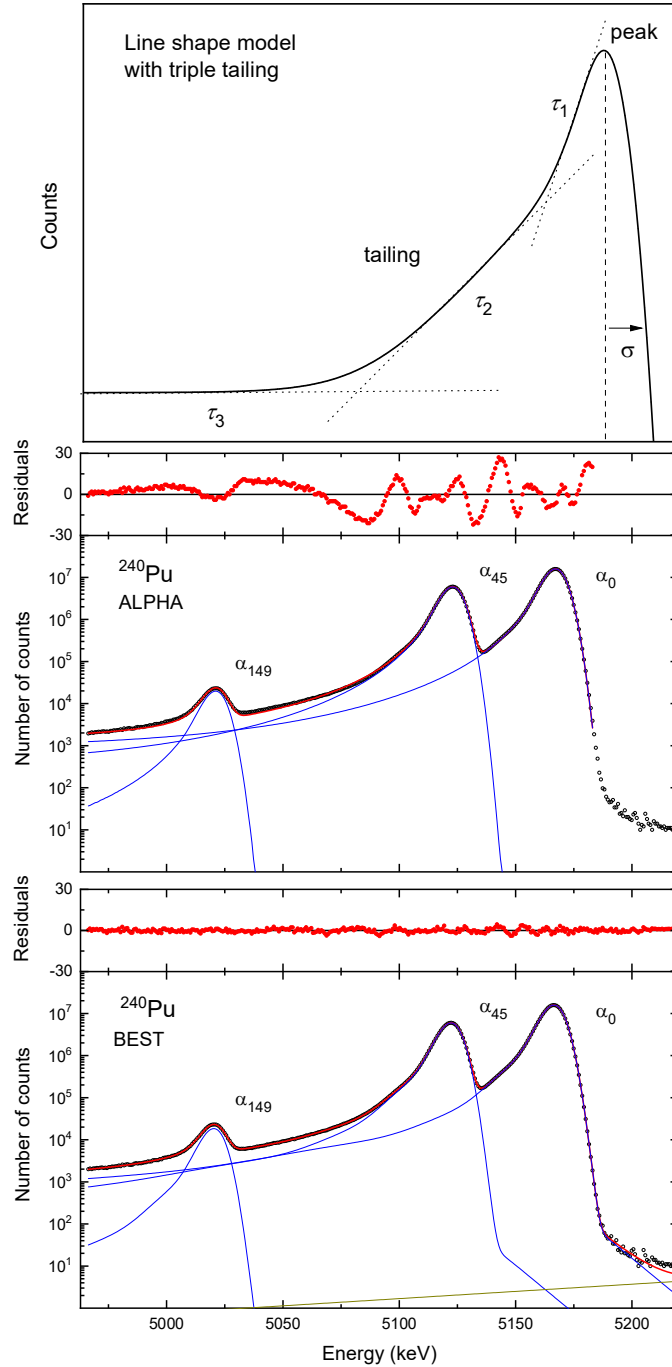


*Figure 21: Top:* Traditional peak shape model based on the convolution of a Gaussian with three exponential tailing functions. *Middle:* Failed peak fit to a  $^{240}\text{Pu}$  alpha spectrum with very high statistical accuracy, using three tailing functions. *Bottom:* Fit of the same  $^{240}\text{Pu}$  spectrum with the 'BEST' shaping model [128].

The methodology has been used to significantly improve the emission probabilities in the decay of  $^{235}\text{U}$  [130],  $^{240}\text{Pu}$  [131, 132],  $^{238}\text{U}$  [133], the  $^{230}\text{U}$  decay series [134], the  $^{225}\text{Ac}/^{213}\text{Bi}$  decay series [39],  $^{236}\text{U}$  [135],  $^{226}\text{Ra}$  [136], and  $^{231}\text{Pa}$  [137]. The published  $^{231}\text{Pa}$  results were the first using direct alpha-particle spectrometry with semiconductor detectors and the values of emission probabilities were improved by an order of magnitude, which should help to solve inconsistencies and inaccuracies in the decay scheme. For  $^{238}\text{U}$ , the thickness of the sources was a trade-off between the conflicting requirements of energy resolution and counting statistics

[138]. Spectra were continuously acquired over a period of 2 years, and an extra-large magnet system had to be used to cover the big  $^{238}\text{U}$  sources. Emission energies and a branching factor for  $^{213}\text{Bi}$  could be improved by removing spectral interferences through chemical separation by collecting recoil atoms on a glass plate [39]. Uncertainty calculations require particular attention to account for correlation effects from interferences and peak shape distortions [122]. Detailed uncertainty budgets were published for the determination of reference values for  $^{226}\text{Ra}$ ,  $^{234}\text{U}$ , and  $^{238}\text{U}$  activity in water in the frame of proficiency tests [139,140].

The energy resolution of silicon-based detectors cannot go below the physical limit of about 8 keV imposed by the finite number of electron–hole pairs that the alpha particle can produce in the Si lattice. These detectors are also imperfect with respect to linearity between pulse height and particle energy, since energy loss in dead layers varies with the particle's energy and the required energy for creating an electron–hole pair depends on the stopping power. More powerful detection techniques are magnetic spectrometers [141], cryogenic detectors [142], and time-of-flight (TOF) instruments [143]. The JRC is constructing the novel 'A-TOF' time-of-flight set-up with focussing magnets to reach a superior energy resolution and linearity (Fig. 22) [144].



*Figure 22: Drs. Krzysztof Pelczar and Stefaan Pommé at the construction of the A-TOF facility, which measures the energy of alpha particles emitted in radioactive decay. The energy resolution is improved by measuring the time-of-flight of the alpha particles over a flightpath of several meters. The aim is to provide accurate nuclear decay data of alpha-emitting nuclides.*

## 4.5 Internal Conversion Coefficients

Together with partners from the STUK (Radiation and Nuclear Safety Authority, Finland), the JRC introduced the use of windowless Peltier-cooled silicon drift detectors for high-resolution internal conversion electron (ICE) spectrometry and demonstrated its potential as an alternative to alpha spectrometry for the isotopic analysis of plutonium mixtures [145,146,147,148,149] (Fig. 23). Whereas in alpha spectrometry the alpha transitions from the fissile isotope  $^{239}\text{Pu}$  are strongly interfered by the transitions of  $^{240}\text{Pu}$  [38,150], in ICE spectrometry the respective L and M+ ICE energies of the Pu isotopes are well separated and ideally suited for isotopic fingerprinting [145,147] (Fig. 24). The 'BEST' deconvolution software [128] is easily adapted to analyse mixed x-ray and ICE spectra in order to determine the relative ICE emission intensities from the fitted peak areas. For the plutonium isotopes  $^{238,239,240}\text{Pu}$ , a good agreement is found with the theoretically expected Internal Conversion Coefficients (ICC) calculated from the Brllc database [147]. On the other hand, the

theoretical ICC values for the 59 keV transition following  $^{241}\text{Am}$  decay were contradicted, since the experimental data are anomalous due to a nuclear penetration effect [148]. These findings contribute to a more reliable data set, complementary to some of the best results obtained with large magnetic spectrometers, and completed with a comprehensive uncertainty budget. All necessary data are in place to use this analytical method for fingerprinting of plutonium mixtures.

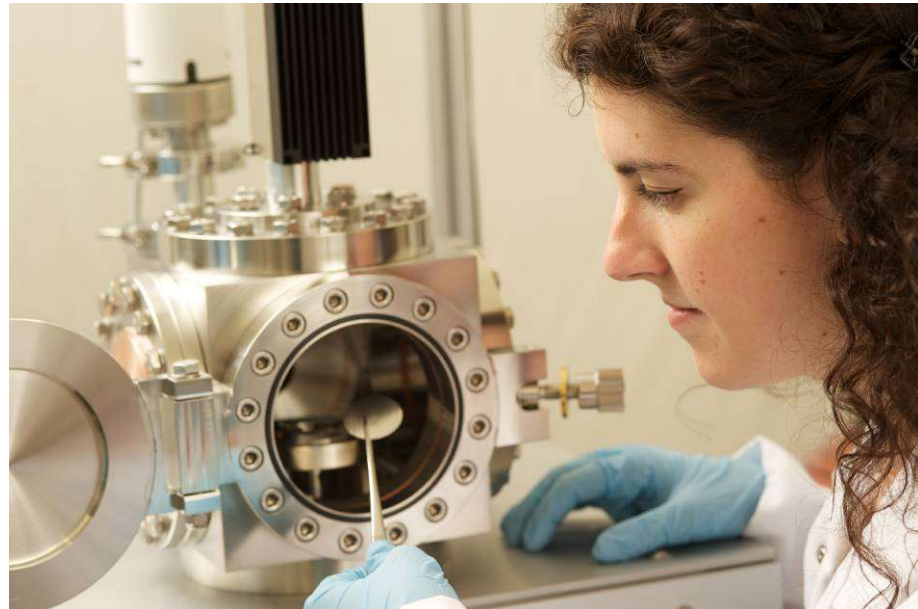


*Figure 23: Visiting scientist Dr. Belén Caro Marroyo introducing a source in the conversion electron spectrometer equipped with a silicon drift detector. She co-developed the 'BEST' spectral analysis software.*

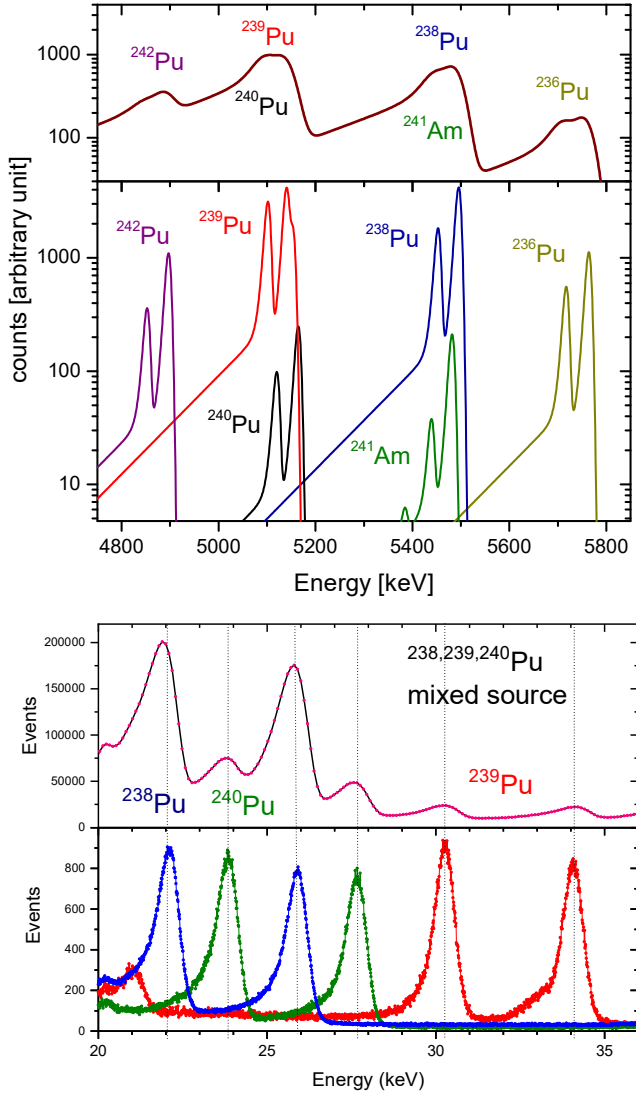


*Figure 24: Top: Model representation of mixed alpha spectra from plutonium isotopes (with low and high energy resolution) [149]. Bottom: Measured L-shell conversion electron spectrum of a mixed plutonium source and individual spectra of  $^{238},^{239},^{240}\text{Pu}$  [146].*

## 4.6 Gamma-ray intensities

Gamma-ray spectrometry is the workhorse of radioanalysis, enabling identification and quantification of a mixture of radionuclides in one spectrum and requiring little effort in sample preparation. In particular, High-purity Ge detectors are routinely used owing to their superior energy resolution for gamma quanta. Their energy-dependent detection efficiency is generally established by fitting a smooth curve through measured count rates per Bq at specific gamma-ray energies from SI-traceable calibration sources, taking into account the  $\gamma$ -ray intensities and the half-life of the corresponding nuclide. Modelling is often used to convert the efficiency curve to different geometries [151]. Accurate decay data are therefore indispensable for the user community to perform SI-traceable activity measurements. Primary standardisation laboratories provide accurate decay data by performing  $\gamma$ -ray spectrometry on calibrated sources. The JRC has published  $\gamma$ -ray intensities of important nuclides in the frame of NORM (naturally occurring radioactive material) [152] and nuclear medicine, such as  $^{235}\text{U}$  [153],  $^{124}\text{Sb}$  [154], and the entire  $^{227}\text{Ac}$  [155] decay chain. A discussion is provided on the choice of proper spectral data for  $^{238}\text{U}$  spectrometry [156].

## 4.7 Cross sections

Production rates of nuclides through nuclear reactions is of great importance in nuclear science (e.g. astrophysics), the safe use of nuclear energy [157], the production of radiopharmaceuticals, and in nuclear techniques for analytical chemistry. Proper calibration of radioactivity measurements is an important aspect in experimental determinations of nuclear cross sections. For example, it was discovered that the cross section for  $^{nat}\text{Hf}(\text{d},\text{x})^{177}\text{Ta}$ , as well as for other reactions producing  $^{177}\text{Ta}$ , was crucially depending on the choice of the  $\gamma$ -ray intensities emitted after the decay of  $^{177}\text{Ta}$  [158]. A misprint in evaluated data lead to an error by a factor of 3. Primary techniques can help to improve accuracy, for example by using  $4\pi \gamma$  counting of a gold neutron fluence monitor in a NaI well detector to underpin the neutron capture cross section of  $^{235}\text{U}$  [159]. The GELINA linear accelerator facility at the JRC produces bunches of neutrons and uses time-of-flight to determine the energy of the neutrons inducing nuclear reactions in a remote experimental set-up along a flightpath. For example, neutron-induced ternary fission particles were measured in a  $\Delta E$ - $E$  detector set-up [160] and the evidence showed that the ternary-to-binary fission ratio was invariable among the resonances in the  $^{235}\text{U}(\text{n},\text{f})$  cross section [161].

## 4.8 $k_0$ factors

In neutron activation analysis (NAA),  $\gamma$ -ray spectrometry is performed on a matrix that has been irradiated by neutrons from a nuclear research reactor with the aim of determining the concentration of elements in the material. The method heavily depends on a combination of nuclear data, including isotopic abundances, neutron capture cross sections and photon intensities. To reduce the combined uncertainty of such factors, Simonits and De Corte aggregated them into a universal constant – the ‘ $k_0$  factor’ – which is determined directly for each relevant  $\gamma$ -ray by analysing a reference material relative to a co-irradiated gold neutron flux monitor [162,163]. The meaning of the  $k_0$  factor was explicitly defined for 17 activation-decay schemes, together with the matching Bateman equations for the time dependence of the generated activity.

Pommé et al. generalised the  $k_0$ -NAA formalism to extreme activation and measurement conditions [163]. Generalised activation-decay equations were derived, with inclusion of burnup effects and successive neutron capture in high-flux regimes, backward branching or looping, in-situ measurements, consecutive irradiations, and mathematical singularities [94]. The  $k_0$ -NAA activation-decay formulas for high-flux conditions were redefined in a compact manner that closely resemble the classical NAA formulas. At high neutron densities, the direct applicability of the  $^{197}\text{Au}(\text{n},\gamma)^{198}\text{Au}$  reaction as a neutron flux monitor is disrupted by the high neutron capture cross section of the reaction product  $^{198}\text{Au}$ . A simple mathematical solution was presented to determine the ensuing burnup effect prior to any characterisation of the neutron field, merely based on the spectrometry of the induced  $^{198}\text{Au}$  and  $^{199}\text{Au}$  decay gamma rays [164,165]. Thus, an iterative procedure for neutron flux monitoring can be avoided.

The Belgian Nuclear Research Centre (SCK CEN) and the JRC set up a joint NAA laboratory at the BR1 reactor of the SCK [166,167,168]. The data analysis was done in SCK’s  $\gamma$ -ray spectrometry service, which routinely performed environmental monitoring and health physics measurements [169,170,171,172]. A comprehensive uncertainty budget was presented to bring the  $k_0$ -NAA method under statistical control [173]. The content of various reference materials was analysed, among which Al-Co, Al-Au, Al-Ag, and Al-Sc alloys, bronzes, mussel tissue, bovine liver, Antarctic krill, incineration ash, aerosol filters, and water. The SCK CEN performed additional NAA measurements for external clients. The irradiation and measurement conditions for a specific sample were chosen by means of a deterministic simulation tool that quickly predicted spectral shapes and detection limits, which was helpful to reduce interfering activity and to optimise the analytical power [174].

At the fast irradiation facility of the BR1, a series of measurements were performed to improve the  $k_0$  factors and related data for ten analytically important reactions leading to the short-lived radionuclides  $^{20}\text{F}$ ,  $^{71}\text{Zn}$ ,  $^{77m}\text{Se}$ ,  $^{80}\text{Br}$ ,  $^{104}\text{Rh}$ ,  $^{109m}\text{Pd}$ ,  $^{110}\text{Ag}$ ,  $^{124m1}\text{Sb}$ ,  $^{179m}\text{Hf}$ , and  $^{205}\text{Hg}$  [175]. Work was done to improve the  $k_0$ -factor and various associated nuclear data for the 555.8 keV gamma-ray of the  $^{104m}\text{Rh}$ - $^{104}\text{Rh}$  parent-daughter pair, involving adaptations with respect to the activation-decay type and true-coincidence effects [176]. An investigation was made of the  $^{97}\text{Zr}$  half-life value and the  $k_0$  and  $Q_0$  factors for Zr isotopes, which are important monitors for epithermal neutron flux [177]. All these reference values are applicable at other  $k_0$ -NAA laboratories, provided that the applied convention for the characterisation of the neutron field is valid.

## 4.9 Fission product yields

The nuclear fission process was discovered by chemical means when Hahn and Strassmann (1939) identified the elements barium and lanthanum amongst the products resulting from the neutron irradiation of uranium. Applying the drop model to the heavy uranium nucleus, Meitner and Frisch realised that an elongation of the nucleus could lead to a dumbbell shape which would snap into two fragments that recoil away in opposing directions, carrying away a large amount of kinetic energy. Salient features of the fission fragments are asymmetry in their sizes due to favourable nuclear shell effects [178,179,180,181,182,183,184,185], and even-odd staggering in their proton yields reminiscent of the proton pairing in an even-even fissioning nucleus [185,186,187]. One of the big questions about fission dynamics is how much of the motion energy of the elongating nucleus on its path towards neck rupture is transferred to thermal excitation of the nucleons through internal friction.

The fissioning nucleus has to pass a potential energy barrier, as the initial deformation requires energy, whereas at further elongation the Coulomb repulsion provides potential energy. At the scission point, the Q value of the fission process is in large part bound as potential energy through deformation and Coulomb energy, but there is an additional amount of energy free for excitation of collective or intrinsic degrees of freedom. In a model where friction is invoked, the nucleus will arrive thermally excited at the scission point and the bonds between nucleon pairs will be broken. In an adiabatic model, the nuclear viscosity is negligibly small and nucleon pairing persists up to scission. Through the abrupt snapping of the neck, pair breaking may still occur. Thus, a study of the preponderance of fission fragments with even nuclear charge number can render unique insights in the viscosity of cold nuclear matter, i.e. the coupling between the collective motion of the fissioning nucleus and the intrinsic single-particle degrees of freedom of the nucleons.

Physical methods to measure mass, charge, and energy of the fragments require complicated mass separators, such as e.g. the Lohengrin facility at the ILL in Grenoble. However, the mass and charge distributions of the heavy fragments are also accessible through common radioanalytical techniques. Since the fission fragments are in excess of neutrons, they promptly emit some neutrons and undergo isobaric decay with emission of characteristic gamma rays. Gamma-ray spectrometry of the fission products provides their individual yield and an unequivocal identification of their mass and charge numbers. At the 15-MeV linear accelerator of the University of Ghent [188,189], fission of  $^{238}\text{U}$  was induced by bremsstrahlung at seven excitation energies close to the fission barrier [185,186]. Irradiated  $^{238}\text{U}$  samples were transported with a rabbit system, back and forth between the irradiation site and a  $\gamma$ -ray spectrometer, to measure the yield of the short-lived fission products. Long-lived fragments were caught in aluminium foils [190] and measured at longer duration. Some elements were isolated by chemical separation to reduce spectral interference. As part of the radioanalytical process, a set of 'best' nuclear decay data were selected for 118 radionuclides, in particular half-lives and gamma-ray emission probabilities, since some data appeared to be inconsistent with the observations in the experiment [185].

In addition to the radioanalytical work, double energy measurements of the fission fragments were performed with two opposing surface barrier detectors [181]. By combining the results from both techniques, it was possible to derive neutron emission probabilities as well as the mass, charge, and kinetic energy of the fragments at the moment of scission. The study showed the same, very pronounced proton odd-even effect as long as the excitation energy of the nucleus remained below the height of the fission barrier plus the pairing gap, i.e. the energy needed to break up a proton pair [186] (Fig. 25). At the same time, the added excitation energy appeared as increased kinetic energy of the fragments [181]. When the excitation energy was further increased above the pairing gap, the odd-even effect collapsed (Fig. 26) and the kinetic energy dropped as the fragments gained internal heat. This suggests that low-energy fission is a superfluid process with little or no dissipation of collective energy to quasi-particle excitations while the nucleus elongates towards the scission point.

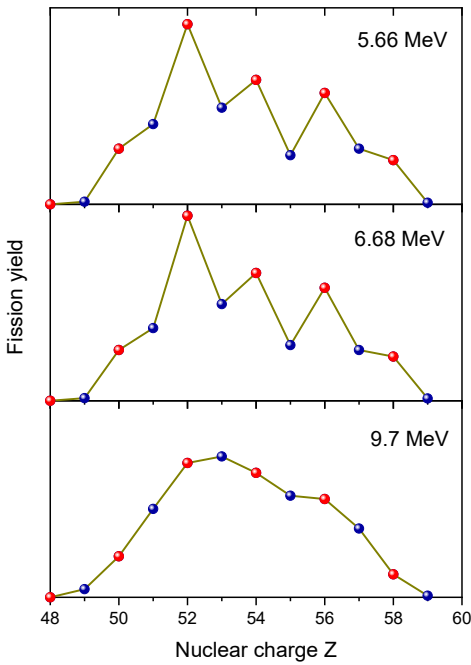


*Figure 25:* Charge distribution of the heavy fission products from bremsstrahlung-induced photofission of  $^{238}\text{U}$  at three average excitation energies, measured by  $\gamma$ -ray spectrometry of the decay products. The odd-even effect disappears when the excitation energy supersedes the pairing gap at the fission barrier.

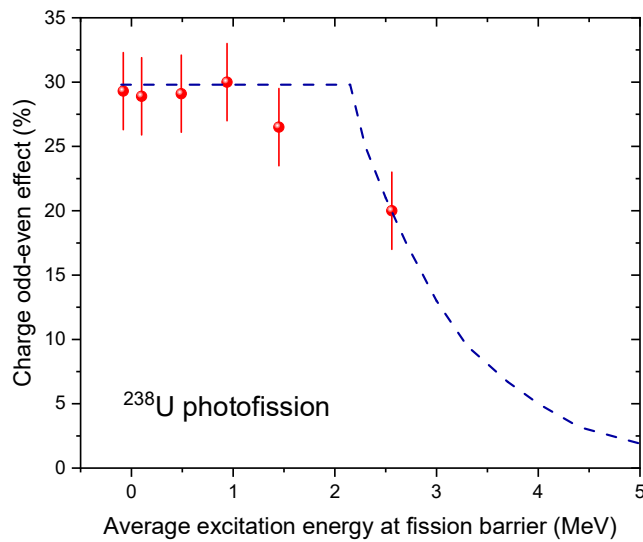


*Figure 26:* Measured fragment charge odd-even effect as a function of the average excitation energy of  $^{238}\text{U}$  at the fission barrier [186]. The line represents a deconvolution of the data accounting for the continuous energy distribution of the bremsstrahlung used for excitation. The odd-even effect drops near the pairing gap at 2.2 MeV.

## 5 The time dimension

### 5.1 The exponential-decay law

In 1900, Rutherford [191] described how activity emanating from thorium decayed away with a constant rate  $\lambda$  such that the ionisation current halved every minute. Today, the 'emanation' can be identified as the noble gas  $^{220}\text{Ra}$ , and the above paper by Rutherford as the first in which the exponential-decay law is explicitly derived to describe the time dependence of radioactive decay. Mathematically, the invariability of the decay constant  $\lambda$  is a necessary as well as a sufficient condition for exponential decay. The decay constants are specific to each radionuclide and inversely proportional to the half-life [95]. The exponential-decay law is a cornerstone of nuclear physics, the common measurement system of radioactivity, and numerous applications derived from it, including radiometric dating and nuclear dosimetry. It also follows directly from quantum theory and its validity has been amply confirmed by experiment [192].

To Rutherford's surprise, the exponential-decay law seemed valid only when measuring in a closed system, since 'the movement of the air caused by the opening or closing of a door at the end of the room opposite to where the apparatus is placed, is often sufficient to considerably diminish the rate of discharge' [191]. More than a century later, the stability of the measurement conditions is still the most critical issue in a debate on the validity of the exponential-decay law. There is a long bibliography from authors who have questioned the invariability of nuclear decay constants based on observed instabilities in certain series of decay rate measurements [193]. Contrary to the notion of radioactive decay as a spontaneous process, new hypotheses were put forward in which solar neutrinos, cosmic neutrinos, gravitation waves, cosmic weather, etc. are actors influencing the radioactive decay process. Common denominators to the claims of violations of the exponential-decay law are the poor metrology on which they are based, the lack of an uncertainty evaluation of the attained experimental stability, and a cognitive bias towards facts contradicting the proposed conjecture.

Most of these claims of new physics have been convincingly invalidated by high-quality metrology showing invariability of the decay constants such that the discussion is largely settled [194,195,196,197,198,199,200,201,202,203,204,205,206]. However, it was unsettling to experience that some editors from reputed journals accepted to publish such highly speculative and spectacular claims, while opposing papers with metrological evidence contradicting those claims. The problem lies not in the liberty taken to suggest new ideas, but in the lack of scrutiny to put these ideas to the test. In the words of Carl Sagan [207]: "At the heart of science is an essential balance between two seemingly contradictory attitudes – an openness to new ideas, no matter how bizarre or counterintuitive they may be, and the most ruthlessly sceptical scrutiny of all ideas, old and new. This is how deep truths are winnowed from deep nonsense."

### 5.2 The 5<sup>th</sup> force

Incomplete uncertainty assessment has a direct impact on science and decision making. The controversy about violations of the exponential-decay law was fed by incomplete uncertainty budgets in measured decay curves with cyclic deviations at the permille level. New theories with high aspirations – involving a 5<sup>th</sup> force! – were proposed to claim that decay is induced by solar and cosmic neutrinos. Consequently, decay constants would not be fixed values – as believed for more than a century – but variables sensitive to changes in neutrino flux. Patents were issued to use repeated beta decay measurements as an alternative to elaborate solar neutrino flux monitoring experiments. Others patented methods to reduce radioactive waste by shortening the half-lives of long-lived nuclides. Questions were raised about the validity of nuclear dating in archaeology and geo- and cosmochronology. The very foundation of radionuclide metrology was affected, since direct comparison of activity measurements is made possible through normalisation to a reference date via the exponential-decay law. Establishing international equivalence of standards for the SI-derived unit becquerel implicitly assumes the invariability of the decay constants, and therefore would require an adjustment if radioactivity would be sensitive to variations in neutrino flux through solar dynamics and the Earth-Sun distance.

The CCRI(II) initiated a large-scale investigation on the most extensive set of long-term activity measurements supplied by 14 metrology institutes across the globe, together spanning a period of 60 years. Analysis of more than 70 decay curves for annual oscillations showed that there was no mutual correlation in the cyclic deviations from exponential decay [41,194,195,196,197,198,204]. This contradicts the assertion that decay rates follow the annual cycle of the solar neutrino flux due to the varying Earth-Sun distance. The most stable data sets had negligible deviations of the order of 0.0006%, thus confirming the invariability of

the decay constants down to that level. On the other hand, environmental effects, such as humidity, temperature, and radon in air, had caused some of the observed cyclic effects in activity measurements.

Reanalysis of the often-cited ‘sinusoidal’ instability in  ${}^3\text{H}$  decay measurements by Falkenberg revealed that the shape of this artefact was caused by the introduction of an arbitrary ‘correction’ function to the data to account for the ‘degradation’ of the poorly executed experiment [196]. The annual cycle in ionisation chamber measurements of a  ${}^{226}\text{Ra}$  source at the PTB in the period 1983–1998 was in phase with radon emission rates in the laboratory, which may have caused a discharge effect in the capacitor. When a new current measurement method was introduced at the PTB in 1999, this annual cycle disappeared and a new, smaller cyclic effect was observed in phase with ambient humidity and temperature [195,208]. The oscillations in the  ${}^{32}\text{Si}$  and  ${}^{36}\text{Cl}$  decay rate measurements at Brookhaven National Laboratory and Ohio State University, respectively, show a strong correlation with the dew point in a nearby weather station [203]. Radon decay rates in a closed vessel in Israel were clearly influenced by weather conditions, such as solar irradiance and rainfall [199,200,201]. Ambient humidity has been identified as the culprit for instabilities in several experiments, considering that it also penetrates temperature-controlled laboratories [209]. Figure 27 shows a correlation plot of  ${}^{134}\text{Cs}$  activity measurements in JRC’s IC1 ionisation chamber with outdoor humidity.

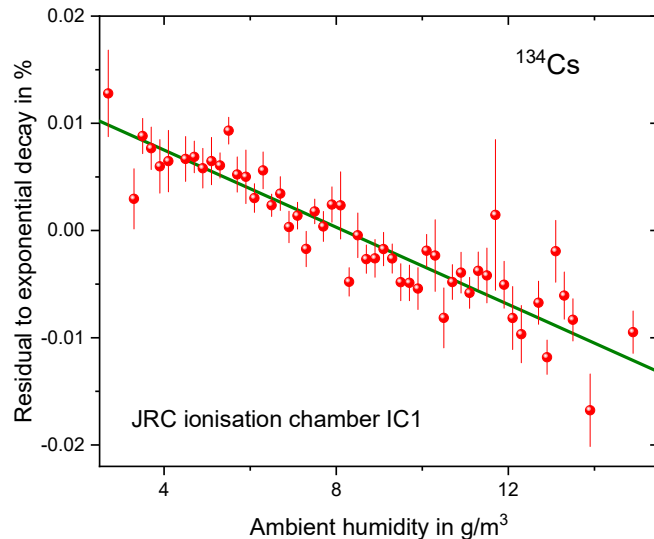


*Figure 27: Average values and standard uncertainty of residuals to exponential decay of  ${}^{134}\text{Cs}$  in JRC’s ionisation chamber IC1 in Geel, Belgium binned as a function of ambient humidity obtained from a weather station in Antwerp at about 40 km distance [210]. Humidity causes an annual cycle in the data.*

Further claims were made of monthly oscillations in decay curves, allegedly associated with rotation of the solar interior. In this type of research, the Lomb-Scargle periodogram is a commonly used statistical tool to search for periodicity in unevenly sampled time series [211]. Whereas the original Lomb-Scargle solution is equivalent to an unweighted fit of a sinusoidal curve to the time series, the equations have been upgraded to apply statistical weighting of data and to allow for fitting a baseline value. Different statistical significance criteria should be applied for cyclic modulations fitted to time series using any of the four options, i.e. weighted or unweighted fitting with or without a free baseline [211]. Applying proper uncertainty propagation, it was found that the claimed monthly ‘solar-neutrino induced decay’ cycles were not statistically significant or else caused by terrestrial weather [192,200,201] (Fig. 28).

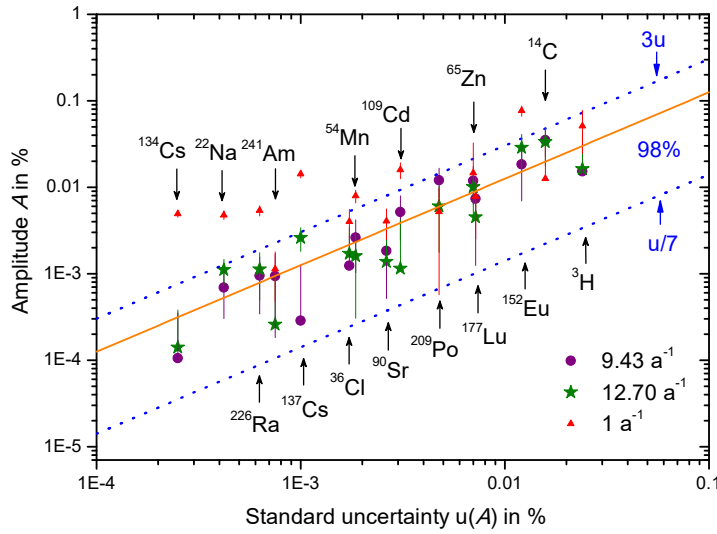


*Figure 28: Amplitudes of annual ( $1 \text{ a}^{-1}$ ) and monthly ( $9.43 \text{ a}^{-1}, 12.7 \text{ a}^{-1}$ ) sinusoidal cycles fitted to the residuals from exponential decay of various nuclides as a function of the uncertainty on the amplitude. The dotted lines correspond to 1% probability for outliers at the low and high side of the associated Rayleigh statistical distribution of random noise. The data were not corrected for environmental influences, which explains the presence of significant annual cycles.*

Some authors apply data dredging methods to propose unsubstantiated claims of causality between correlated variables. For example, repeated measurements of activity and the capacitance of a cable (and even umbilical cord blood parameters) have been associated with space weather variables, whereas the sign of the correlation changed from one measurement to the other. The most likely explanation is susceptibility of the measurements to ambient humidity, which correlated positively with all data sets [202,205]. In conclusion, the claims of new physics are founded on the quicksand of poor metrology. The exponential-decay law remains the solid foundation of the common measurement system of radioactivity and requires no amendment for its application.

### 5.3 Radiochronometry

Relativity theory has done away with the intuitive concept of time being something that flows uniformly and equally through the universe, in the course of which all events happen [212,213]. Events are not crisply ordered in past, present and future, only vaguely ordered in sequence of events. There is no ‘present’ that is common to the universe. Local time proceeds slower when moving fast or being close to a massive object. The illusion of a common time in our everyday life can only be applied as an approximation at close proximity. The value of a nuclear half-life pertains to the conditions in which it was measured, which is by default at rest on the surface of Earth. In this context, half-lives can be considered invariable. Even the world depicted by relativity theory is an approximation, since the world is a quantum one with processes that transform physical quantities from one to the other. There is no special variable ‘time’, the variables evolve with respect to each other. Time in physics is defined by its measurement: time is what a clock reads. Any repetitive process can be used as a clock, the harmonic motion of a pendulum, the position of the sun in the sky, or transitions between the two hyperfine levels of the ground state of a  $^{133}\text{Cs}$  atom.

Radiochronometry is based on the statistical laws ruling the temporal dependence of the expected number of radioactive atoms in a decay chain, commonly known as the Bateman equations [94]. Radioactivity provides unique clocks by which the geological timescale can be calibrated. Before the discovery of radioactive decay, the age of Earth was estimated as only tens of millions of years, based on the time needed for a molten globe to cool down to Earth’s current state. Now it is understood that the heat from radioactive elements present in the composition of Earth has kept its interior hot for billions of years. The inventory of remaining radionuclides stemming from Earth’s original accretion contains only long-lived nuclides ( $>10^8 \text{ y}$ ), since the

shorter-lived nuclides have decayed away. This provides a measure of the time scale at which the synthetic events that created the material of the Solar system stopped.

Age dating through the exponential decay of a radionuclide and the ingrowth of its progeny in a closed system can be achieved in various ways [95], either through the ratio of the atomic concentration of the nuclide at different times (e.g. carbon dating), the ratio of progeny to parent nuclides (e.g. uranium-lead dating), or isochron dating methods which apply a ratio with a stable isotope to gain independence from initial amounts of the progeny (e.g. lead-lead and rubidium-strontium dating). The dating equations are linearly proportional to the half-life of the parent or on the ratio of the half-lives involved, which means that the relative uncertainty of the half-life constitutes an upper limit to the attainable accuracy on the age. Owing to the accuracy attainable with mass spectrometry techniques, the half-life uncertainty has become a potential bottleneck in the uncertainty budget of nuclear chronometry.

The most commonly used nuclear chronometers are mathematically equivalent to a singular parent-progeny decay, for which the derivation of the dating equation is straightforward. However, the formulas for the uncertainty propagation were considered difficult to derive and therefore sometimes addressed by simulation methods. Recently, succinct but rigorous mathematical solutions were published for nuclear dating by atom ratio (mass spectrometry) and activity ratio (nuclear spectrometry) measurements of parent-progeny pairs [95,214]. In addition, approximating formulas were presented that showed that, in certain conditions, the propagation factors of relative uncertainties on measured ratios and decay constants towards the age can approach unity, but also large or small numbers are possible [214]. An important observation is that radiometric dating through atom ratio measurements is less sensitive to the progeny half-life and through activity ratio measurements less sensitive to the parent half-life. Activity ratio measurements enhance the signal of the short-lived nuclide, and may be a good alternative to atom ratio measurements in cases where the atom concentration of the short-lived nuclide is particularly low.

Besides cosmo- and geochronology, an important application is found in nuclear forensics, where the age of a nuclear material refers to the elapsed time since the most recent chemical separation of a radionuclide from its decay products. At a shorter timescale, precise dating of an underground nuclear explosion can be achieved through spectrometry of released fission products captured by environmental monitoring networks. Specific unbiased equations have been presented for  $^{95}\text{Zr}$ - $^{95}\text{Nb}$  chronometry of a nuclear event [215], which is complicated by a decay branch passing through a meta-stable state,  $^{95\text{m}}\text{Nb}$ . An additional complication arises when the duration of the activity measurement is not infinitely short compared to the half-lives of the nuclides involved. In that case, extended uncertainty formulas should be used that include the uncertainty on the decay during the measurement [216]. This has been demonstrated for the  $^{140}\text{Ba}$ - $^{140}\text{La}$  chronometer used in the frame of the International Monitoring System (IMS) for the verification of the Comprehensive Nuclear Test-Ban Treaty (CTBT), as well as the medically important alpha-emitting decay chain of  $^{227}\text{Th}$ - $^{223}\text{Ra}$  (Figs. 29 and 30) when used for targeted radiotherapy of lymphoma cells. The age of the  $^{227}\text{Th}$ - $^{223}\text{Ra}$  pair is needed for activity calibration in ionisation chambers, since the induced ionisation current depends on their evolving activity ratio with time [217].

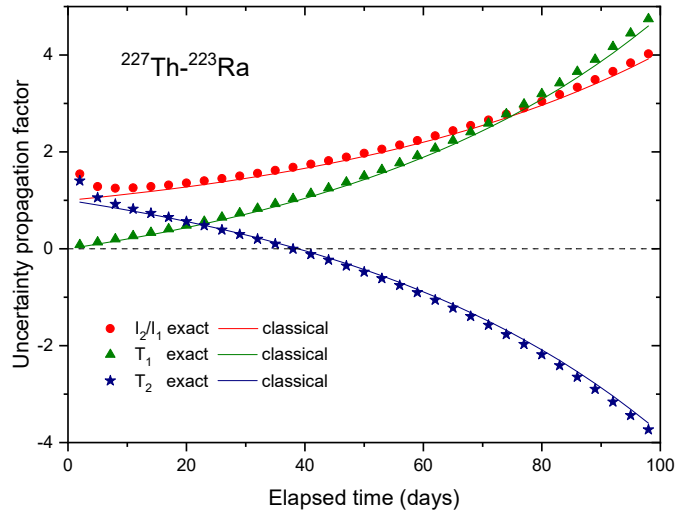


*Figure 29: Uncertainty propagation factors of the activity ratio and the parent and progeny half-lives towards radiochronometry for hypothetical measurements of two days. The exact formula (symbols) is compared to the classical formula (lines) in which decay during the measurement is not taken into account [216].*

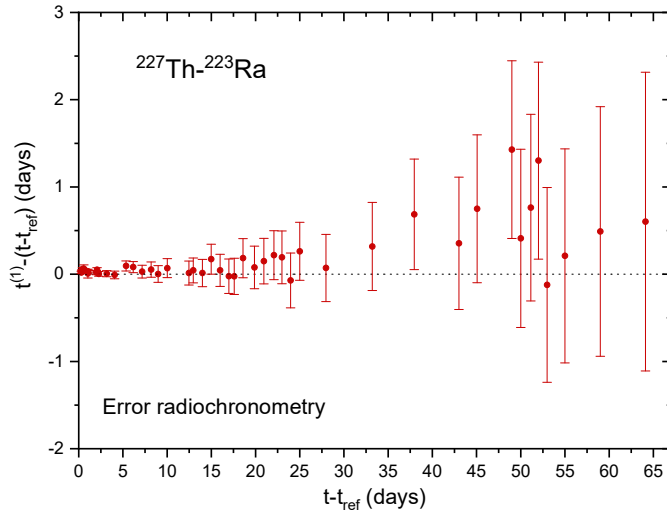


*Figure 30: The achieved statistical control over the residuals of  $^{227}\text{Th}$ - $^{223}\text{Ra}$  radiochronometry results using HPGe detectors at the NPL [216]. On the x-axis is the time of measurement relative to the moment of chemical separation of  $^{227}\text{Th}$  from its progeny. The y-axis shows the error of the calculated separation date through radiochronometry, which was mostly within the calculated standard uncertainty.*

## 5.4 Renewal processes

Radioactive decay is a stochastic process at the level of single atoms. It is impossible to predict when a particular atom will decay regardless of how long the atom has existed. Its survival probability takes the shape of an exponential. Applied to a large number of atoms with the same half-life, the number of remaining atoms as well as the activity decreases exponentially with time. As a result of the randomness of

decay, the time intervals between successive decays follow an exponential distribution and non-selective counting of decays is governed by Poisson statistics. The Poisson process is the most important of all renewal processes, owing to the memoryless property of the exponential interarrival distribution. Other renewal processes apply in the practice of nuclear counting and the variance of their arrival times will eventually determine the counting statistics [3,218,219,220,221,222,223]. Since a renewal process is independent of its history, the interval time between  $k$  successive events is obtained from a  $k$ -fold self-convolution of the single time-interval density. Laplace transforms are useful to study those processes, to convert convolutions in the time domain into multiplications in Laplace space.

When a nuclear detector observes a random fraction of the decays of a radioactive source, e.g. through ‘statistical thinning’ determined by the solid angle covered by the sensitive detector volume, the time series of the detected decays is a new Poisson process. The probability distribution of the number of counts within a short time interval is governed by Poisson statistics. This applies in stationary conditions, i.e. in so far as only a negligible fraction of the source has decayed away in the course of measurement. Nuclear counting devices need a characteristic amount of time to process an incoming signal, and remain irresponsible to successive signals during that time. It is called ‘non-extending dead time’, when the system resumes its task as soon as the pulse is processed. A system has ‘extending dead time’ if its dead-time period is prolonged by the arrival of a new event. Authoritative books have erroneously claimed that all nuclear counters can be described by one of these two types, or by a combination of them. However, this does not account for the statistical effects caused by pulse pileup, which is the main loss mechanism in contemporary spectrometry chains [219,220,224] (Fig. 31).

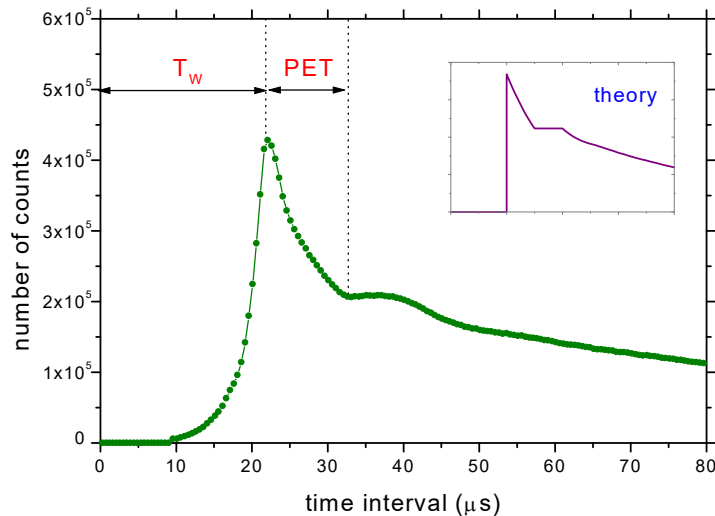


*Figure 31: Measured and theoretical time-interval spectrum in a  $\gamma$ -ray spectrometer with pileup rejection, which is the main count loss mechanism [220].  $T_w$  is the pulse width and PET the width of the rising edge of the pulse.*

## 5.5 Counting statistics

In the 20<sup>th</sup> century, extensive pioneering work was done to gain control over nuclear counting statistics in primary standardisation techniques, including complex formulas applicable to coincidence counting [47]. Live-time counting is performed with a single-channel system on which a known extending or non-extending dead time is imposed that exceeds the pulse width of the detector signals [2,3]. This principle can also be applied by software in the off-line analysis of list-mode files obtained with digital data acquisition methods. At moderate count rates, the recorded real-time to live-time ratio is an accurate correction factor for the incurred count loss.

At high count rates, the live-time technique has to be corrected for a secondary effect due to the finite width of the detector pulses. A pulse occurring at the end of an imposed non-extending dead time interval may block a partly overlapping event outside the dead time period that would normally be counted, thus inadvertently causing additional count loss. In the case of an extending dead time, only well-separated pulses prolong the system dead time, while piled-up pulses do not. In this case, the system throughput will be slightly higher than expected. This phenomenon has been studied in the time dimension as a series arrangement of two dead times, and exact equations for the throughput were derived from the time interval distributions [223,225,226]. A noticeable cascade effect has also been observed in mass spectrometry at high count rate at the JRC, however this aspect is not yet common knowledge in the mass metrology community. The problem can be solved technically by extending the dead time period with a logical OR over the entire width of each incoming pulse.

Other secondary effects occur when the nuclear half-life is not infinitely long compared to the measurement time, since the exponential change of the decay rate has an effect on the throughput and counting statistics [3]. Firstly, the distribution law of the expected number of counts in a measurement deviates from a Poisson process [227]. More importantly, live-time counting techniques are biased towards low values when correcting for the count loss of short-lived radionuclides in a non-stationary regime, since on average they emphasise the time regions with low input rate. This problem has been observed with reference measurements of short-lived PET nuclides in the SIRTI transfer instrument of the BIPM. Practical throughput correction formulas have been derived for the case in which the total count rate in the detector changes proportionally with the activity of the short-lived nuclide [3,228].

When ‘loss-free counting’ (LFC) [229] was introduced in NAA as a novel adaptive count-loss correction method suitable in non-stationary counting conditions (Fig. 32), an early report stated that statistical control could not be achieved [230]. This problem triggered a rethinking of the count-loss processes in nuclear spectrometry and led to new insights into the statistics induced by pulse pileup in spectrometers. Pulse pileup in a narrow spectral region-of-interest and pileup rejection over the entire energy spectrum cause simultaneous loss of two coincident counts instead of one, which is an effect that cannot be generated by a combination of extending and non-extending dead time. Whereas dead time preserves the asymptotic slope of the incoming exponential time distribution at infinity, the pileup mechanism does not because it combines events from single and multiple interval density functions [220] (Fig. 33). The latter applies also to the time intervals from an incomplete part of the spectrum, even though their counting statistics is closer to Poisson than for the full spectrum [219,220]. Pileup causes a broadening of the count distribution in a live-time interval [231] (Fig. 34) which affects LFC statistics as well [231,232,233,234,235,236,237] (Fig. 35).

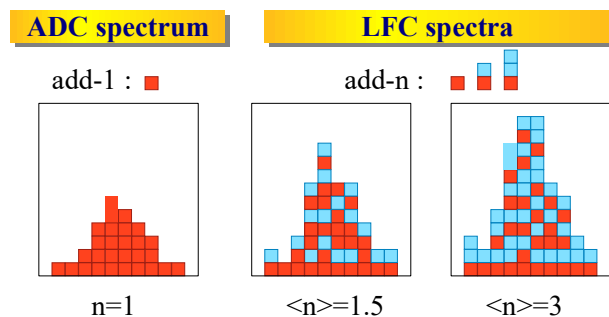


*Figure 32: LFC techniques add virtual counts to the spectrum to compensate for count loss based on the real-time to live-time ratio in short time intervals [229].*

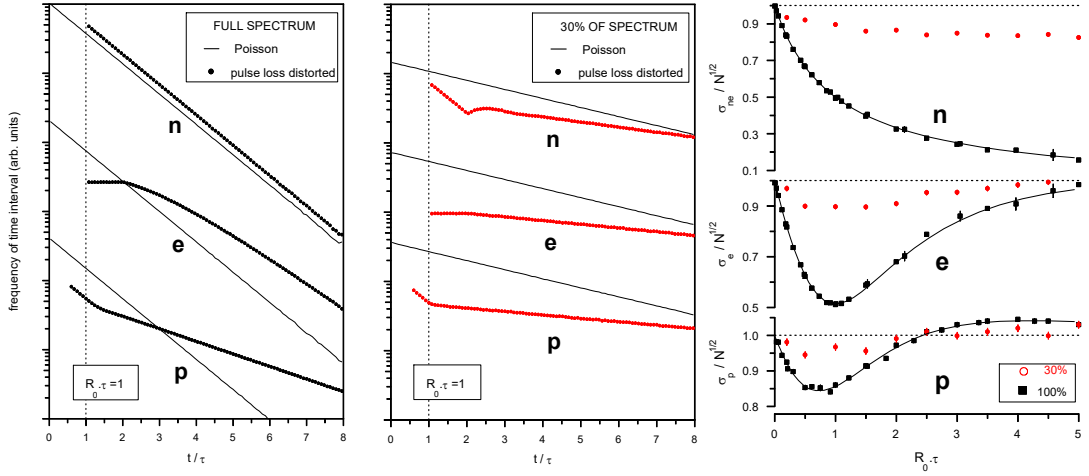


*Figure 33: Left: Time-interval distributions of the full spectrum and a 30% fraction of the spectrum for counters with non-extending dead time, extending dead time, and pileup rejection. Right: Corresponding standard deviation of counting in real time, relative to Poisson uncertainty and as a function of input rate.*

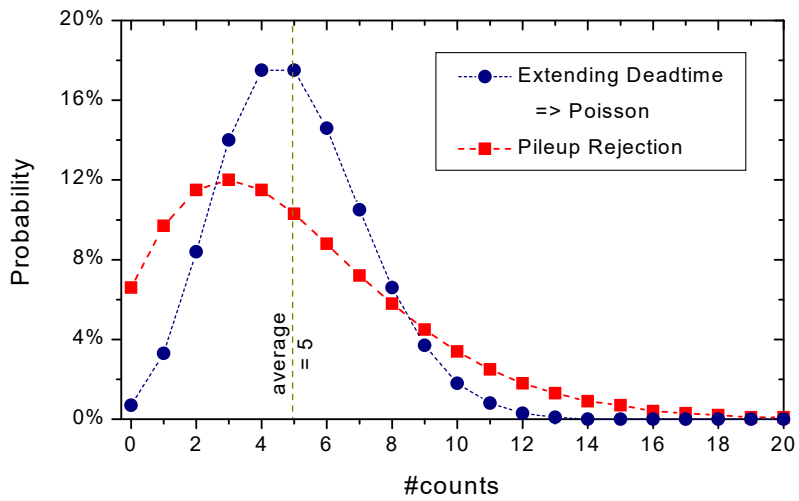


*Figure 34: Broadening of the valid count distribution in a live-time period due to pileup rejection, compared to extending dead time for which Poisson statistics applies [231].*

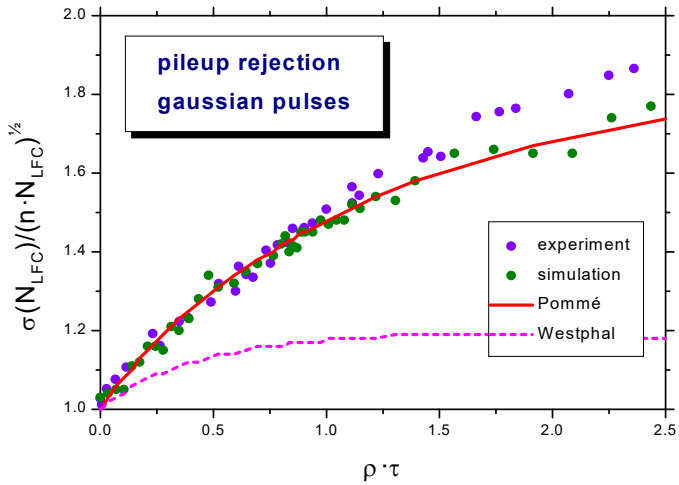


*Figure 35: Deviation of LFC statistical uncertainty from Poisson statistics as a function of input rate, when taking the integral number of events in the full spectrum. For small fractions of the spectrum, the Westphal formula is asymptotically valid.*

Statistical control was eventually achieved over practically any common configuration used for radioanalytical measurement [3,218], from analog (continuously variable) to digital counters, in real time or live time, or by ‘loss-free counting’ and ‘zero dead time’ (ZDT) counting with a variance spectrum. Theoretical calculations were confirmed experimentally by direct comparison with statistical variances in thousands of  $\gamma$ -ray spectra taken with HPGe detectors in different configurations, with classical resistive feedback pre-amplifiers and transistor-reset pre-amplifiers, analog amplifiers with semi-Gaussian pulse shaping or with a gated integrator, systems with and without pileup rejection, fast and slow ADC’s of the fixed dead-time or Wilkinson type, digital counters of different brands, measurements in real-time mode, live-time mode and with LFC or ZDT. Additional evidence was provided through bespoke simulation software, which allowed exploring various count-loss processes, including some not accessible by measurement. The time-interval distributions of successively processed pulses in the counters were studied with a time-interval digitiser [238] and excellent agreement was found with the theoretical predictions for full spectra as well as for regions-of-interest of varying size [220].

## 6 Epilogue

*[...] as we know, there are known knowns; there are things we know we know. We also know there are known unknowns; that is to say we know there are some things we do not know. But there are also unknown unknowns – the ones we don't know we don't know.'*

– Donald Rumsfeld

In spite of the vast theoretical and metrological knowledge on radioactivity accrued over more than a century, there are limits to the detail in which decay characteristics can be modelled or predicted and to the completeness and accuracy of the thousands of decay schemes [4]. Unknown errors reveal themselves as inconsistencies in comparison with other measurement results, possibly in the shape of unexpected variance in repeatability studies, discrepancies among various methods, laboratories, literature data, etc. Absence of such indicators makes us oblivious of hidden sources of error affecting the accuracy of the measurement. They may be tackled by an active search based on reason and completing the metrological puzzle using all possible hints, somewhat comparable to the discovery of dark matter and dark energy in cosmology. Lack of investment into a deeper understanding of every aspect involved leads to over-confidence in the outcome as well as the interpretation of the measurement.

Weapons against overconfidence are in-depth study of the fundamental properties of the measurand, extensive sensitivity analysis, long-term investment in mastering metrological techniques, repeatability tests, redundancy of methods, training, and education [4]. This level of scrutiny in the metrological world serves as an example for science at large. Confidence in radioactivity measurements lays a solid foundation for its countless applications through state-of-the-art radioanalytical methods impacting nuclear science, medicine, health physics, nuclear safety, security, safeguards, forensics, decommissioning, waste management, radiochronometry, geochemistry, geochronology, climate studies, environmental studies, and other forms of fundamental and applied sciences.

## **7 Conclusions**

Measurement science is a key enabler of innovation. Metrology is the arbiter between science and fiction. One could argue that there is no science without measurement. The science of measurement is a science in all fields of sciences. Confidence in science crucially relies on the trustworthiness of the metrology behind it. The hallmark of good metrology lies not merely in the claimed accuracy of the measurement result, but more so in the correct and complete assessment of its uncertainty, that is, understanding and quantifying all underlying sources of measurement error, and ultimately achieving statistical control over the method. The radioanalytical world with its plethora of scientific realisations is supported by a small community of radionuclide metrologists who have dedicated their professional lives to perfecting the art of radioactivity measurement. The house of science stands firmly on the solid foundation of their work.

## 8 References

1. Simpson B, Judge S (Eds) (2007) Radionuclide metrology. Metrologia Volume 44(4)
2. Karam L, Keightley J, Los Arcos JM (Eds) (2015) Uncertainties in radionuclide metrology. Metrologia Volume 52(3)
3. Pommé S (2007) Methods for primary standardization of activity. Metrologia 44:S17-S26
4. Pommé S, Fitzgerald R, Keightley J (2015) Uncertainty of nuclear counting. Metrologia 52:S3-S17
5. Pommé S (2016) When the model doesn't cover reality: examples from radionuclide metrology. Metrologia 53:S55-S64
6. Sibbens G, Altzitzoglou T (2007) Preparation of radioactive sources for radionuclide metrology. Metrologia 44:S71-S78
7. Schrader H (2007) Ionization chambers. Metrologia 44:S53-S66
8. Amiot M-N, Chisté V, Fitzgerald R, Juget F, Michotte C, Pearce A, Ratel G, Zimmerman BE (2015) Uncertainty evaluation in activity measurements using ionization chambers. Metrologia 52:S108-S122
9. Woods MJ, Reher DFG, Ratel G (2000) Equivalence in radionuclide metrology. Appl Radiat Isot 52:313-318
10. Saldarriaga Vargas C, Rodriguez Pérez S, Baete K, Pommé S, Paepen J, Van Ammel R, Struelens L (2018) Intercomparison of  $^{99m}\text{Tc}$ ,  $^{18}\text{F}$ , and  $^{111}\text{In}$  activity measurements with radionuclide calibrators in Belgian hospitals. Physica Medica 45:134-142
11. Saldarriaga Vargas C, et al. (2020) An international multi-center investigation on the accuracy of radionuclide calibrators in nuclear medicine theranostics. EJNMMI Physics 7:69
12. Regan PH, Judge SM, Keightley JD, Pearce AK (2018) Radionuclide Metrology and Standards in Nuclear Physics. Nucl Phys News 28:25-29
13. Judge SM, Regan PH (2017) Radionuclide metrology research for nuclear site decommissioning. Rad Phys Chem 140:463-465
14. BIPM, KCDB (key comparison database), <https://www.bipm.org/kcdb/>
15. Ratel G (2007) The Système International de Référence and its application in key comparisons. Metrologia 44 S7-S16
16. Cox MG, Michotte C, Pearce AK (2007) Measurement modelling of the International Reference System (SIR) for gamma-emitting radionuclides. Monographie BIPM-7, BIPM, Sèvres
17. Michotte C, Nonis M, Bobin C, Altzitzoglou T, Sibbens G (2013) The SIRTI : a new tool developed at the BIPM for comparing activity measurements of short-lived radionuclides world-wide. Rapport BIPM-2013/02, BIPM, Sèvres, France
18. Coulon R, Judge S, Liu Haoran, Michotte C (2021) The international reference system for pure beta-particle emitting radionuclides: an evaluation of the measurement uncertainties. Metrologia 58:025007
19. Working Group 1 of the Joint Committee for Guides in Metrology (2008) Evaluation of measurement data — Guide to the expression of uncertainty in measurement. JCGM 100:2008
20. Working Group 2 of the Joint Committee for Guides in Metrology (2012) International vocabulary of metrology – Basic and general concepts and associated terms (VIM). JCGM 200:2012
21. Pommé S, Keightley J (2015) Determination of a reference value and its uncertainty through a power-moderated mean. Metrologia 52:S200-S212
22. Pommé S, Spasova Y (2008) A practical procedure for assigning a reference value and uncertainty in the frame of an interlaboratory comparison. Accreditation and Quality Assurance 13:83-89
23. Pommé S (2012) Determination of a reference value, associated standard uncertainty and degrees of equivalence —for CCRI(II) key comparison data. JRC Scientific and Policy Reports EUR 25355 EN (EUR—Scientific and Technical Research Series) (doi:10.2787/61338 2012)

24. Supplemental information to Ref. 21: Spreadsheet with PMM algorithm downloadable at the Metrologia website.
25. Pommé S (2006) An intuitive visualisation of intercomparison results applied to the KCDB. *Appl Radiat Isot* 64:1158-1162
26. Spasova Y, Pommé S, Wätjen U (2007) Visualisation of interlaboratory comparison results in PomPlots. *Accred Qual Ass* 12:623-627
27. Jerome S et al (2020) Half-life determination and comparison of activity standards of  $^{231}\text{Pa}$ . *Appl Radiat Isot* 155:108837
28. Jobbágy V, Hult M (2020) Performance evaluation of a European scale proficiency test on radon-in-water measurements in Europe. *Appl Radiat Isot* 160:109111
29. Sobiech-Matura K, Lutter G, Van Ammel R, Marissens G, Emteborg H, Hult M (2020) Evaluation of the 2017 EC Proficiency Test on  $^{131}\text{I}$ ,  $^{134}\text{Cs}$  and  $^{137}\text{Cs}$  in maize powder. JRC Technical Report, EUR 30142 EN, DOI:10.2760/54966
30. European Union (2016) Consolidated version of the treaty establishing the European Atomic Energy Community. ISBN 978-92-824-5144-1, doi:10.2860/45054, Website: <https://www.consilium.europa.eu/en/documents-publications/publications/euratom-treaty/>
31. Denecke B, Sibbens G, Szabo T, Hult M, Persson L (2000) Improvements in quantitative source preparation. *Appl Radiat Isot* 52:351-355
32. Pommé S, Sibbens G (2008) Alpha-particle counting and spectrometry in a primary standardisation laboratory. *Acta Chim Slov* 52:111-119
33. Van Ammel R, Eykens S, Eykens R, Pommé S (2011) Preparation of drop-deposited quantitative uranium sources with low self-absorption. *Nucl Instr Meth A* 652:76-78
34. Lourenço V, Bobin C (2015) Weighing uncertainties in quantitative source preparation for radionuclide metrology. *Metrologia* 52:S18-S29
35. Ingelbrecht C et al. (1999) Electrodeposition of  $^{149}\text{Sm}$  targets for  $(n,\alpha)$  studies. *Nucl. Instr. Meth A* 438:36-39
36. Goeminne G et al. (2002) Preparation and characterisation of an  $^{39}\text{Ar}$  sample and study of the  $^{39}\text{Ar}(n_{th},\alpha)^{36}\text{S}$  reaction. *Nucl Instr Meth A* 489: 577-583
37. Jobbágy V, Crespo M T, Van Ammel R, Marouli M, Moens A, Pommé S, García-Toraño E (2013) Preparation of high-resolution  $^{238}\text{U}$   $\alpha$ -sources by electrodeposition: a comprehensive study. *J Radioanal Nucl Chem* 298/345-352
38. Sibbens G, Altzitzoglou T, Benedik L, Pommé S, Van Ammel R (2008)  $\alpha$ -particle and  $\gamma$ -ray spectrometry of a plutonium solution for impurity determination. *Appl Radiat Isot* 66:813-818
39. Marouli M et al. (2013) Decay data measurements on  $^{213}\text{Bi}$  using recoil atoms. *Appl Radiat Isot* 74:123-127
40. Suliman G et al. (2013) Half-lives of  $^{221}\text{Fr}$ ,  $^{217}\text{At}$ ,  $^{213}\text{Bi}$ ,  $^{213}\text{Po}$  and  $^{209}\text{Pb}$  from the  $^{225}\text{Ac}$  decay series. *Appl Radiat Isot* 77:32-37
41. Pommé S, Stroh H, Van Ammel R (2019) The  $^{55}\text{Fe}$  half-life measured with a pressurised proportional counter. *Appl Radiat Isot* 148:27-34
42. Denecke B, Grosse G, Szabo T (1998) Gain stabilisation of gas-flow proportional counters. *Appl Radiat Isot* 49:1117-1121
43. Johansson L, Sibbens G, Altzitzoglou T, Denecke B (2002) Self-absorption correction in standardisation of  $^{204}\text{Tl}$ . *Appl Radiat Isot* 56:199-203
44. Johansson L, Altzitzoglou T, Sibbens G, Pommé S, Denecke B (2003) Standardisation of  $^{238}\text{Pu}$  using four methods of measurement. *Nucl Instr Meth A* 505:699-706
45. Pommé S, Altzitzoglou T, Van Ammel R, Sibbens G (2021) Standardisation of  $^{241}\text{Am}$  activity for a key comparison. *J Radioanal Nucl Chem* 330:985-996

46. Ratel G, Michotte C, Johansson L, Judge S, Kharitonov I A (2007) Update of the BIPM comparison BIPM.RI(II)-K1.Am-241 of activity measurements of the radionuclide  $^{241}\text{Am}$  to include the 2006 VNIIM result, links for the international 2003 CCRI(II)-K2.Am-241 comparison and links for the 2006 regional comparison COOMET.RI(II)-K2.Am-241G. *Metrologia Technical Supplement* 44:06007
47. International Commission on Radiation Units and Measurements (1994) Particle Counting in Radioactivity Measurements. ICRU Report 52 (Maryland, USA) pp 80
48. Bobin C (2007) Primary standardization of activity using the coincidence method based on analogue instrumentation. *Metrologia* 44 S27-S31
49. Keightley J, Park T S (2007) Digital coincidence counting for radionuclide standardization. *Metrologia* 44:S32-35
50. Fitzgerald R, Bailat C, Bobin C, Keightley J D (2015) Uncertainties in  $4n\beta-\gamma$  coincidence counting. *Metrologia* 52:S86-S96
51. Johansson L, Altzitzoglou T, Sibbens G, Denecke B, Reher D (2003) Six direct methods for standardisation of  $^{152}\text{Eu}$ . *Nucl Instr Meth A* 508:378-387
52. Michotte C, Ratel G, Courte S, Joseph L (2015) BIPM comparison BIPM.RI(II)-K1.Zn-65 of activity measurements of the radionuclide  $^{65}\text{Zn}$  for the BARC (India) with linked results for the CCRI(II)-K2.Zn-65 comparison. *Metrologia* 52:Tech Suppl 06007
53. Michotte C, Courte S, Nonis M, Kossert K, Marganiec-Gałązka J (2020) Update of the BIPM comparison BIPM.RI(II)-K1.Mn-54 of activity measurements of the radionuclide  $^{54}\text{Mn}$  to include the 2017 result of the PTB (Germany) and the linked results from the CCRI(II)-K2.Mn-54 comparison. *Metrologia* 57:Tech Suppl 06005
54. Ratel G, Michotte C (2004) BIPM comparison BIPM.RI(II)-K1.Ir-192 of the activity measurements of the radionuclide  $^{192}\text{Ir}$  and links for the international comparison CCRI(II)-K2.Ir-192. *Metrologia* 41:Tech Suppl 06013
55. Ratel G, Michotte C, Wätjen U, Janßen H, Szücs L, Coursol N, Hino Y (2005) Activity measurements of the radionuclide  $^{134}\text{Cs}$  for the IRMM, Geel, PTB, Germany, OMH, Hungary, LNE-LNHB, France and the NMIJ, Japan in the ongoing comparison BIPM.RI(II)-K1.Cs-134. *Metrologia* 42, Tech Suppl 06009
56. Ratel G, Michotte C, Hino Y, Wätjen U (2005) Activity measurements of the radionuclide  $^{137}\text{Cs}$  for the NMIJ, Japan and the IRMM, Geel in the ongoing comparison BIPM.RI(II)-K1.Cs-137 and update of the KCRV. *Metrologia* 42, Tech Suppl 06009
57. Pommé S, Altzitzoglou T, Van Ammel R, Sibbens G (2005) Standardisation of  $^{125}\text{I}$  using seven techniques for radioactivity measurement. *Nucl Instr Meth A* 544:584-592
58. Pommé S, Altzitzoglou T, Van Ammel R, Sibbens G (2005) Erratum to "Standardisation of  $^{125}\text{I}$  using seven techniques for radioactivity measurement": [Nucl. Instr. and Meth. A 544 (2005) 584-592] Nucl Instr Meth A 555:459
59. Chauvenet B (2010) International exercise on  $^{124}\text{Sb}$  activity measurements. *Appl Radiat Isot* 68:1207-1210
60. Thiam C, Bobin C, Maringer F J, Peyres V, Pommé S (2015) Assessment of the uncertainty budget associated with  $4\pi\gamma$  counting. *Metrologia* 52:S97-S107
61. Pommé S (2009) Detection efficiency calculation for photons, electrons and positrons in a well detector; Part I: Analytical Model. *Nucl Instr Meth A* 604:584-591
62. Pommé S, Sibbens G, Vidmar T, Camps J, Peyres V (2009) Detection efficiency calculation for photons, electrons and positrons in a well detector; Part II: analytical model versus simulations. *Nucl Instr Meth A* 606:501-507
63. Pommé S, Camps J, Sibbens G, Spasova Y (2009) Some modifications to Sima's model for total efficiency calculation of well-type photon detectors. *J Radioanal Nucl Chem* 281:143-147
64. Pommé S (2012) STEFFY – Software for calculation of nuclide-specific total counting efficiency in well-type  $\gamma$ -ray detectors. *Appl Radiat Isot* 70:2070-2074

65. Kossert K, et al (2014) Results of the EURAMET.RI(II)-K2.Ho-166m activity comparison. *Metrologia* 51:Tech Suppl 06022
66. Wallner A, Schillebeeckx P, Pommé S, Wagemans J, Heyse J, Capote-Noy R, Froehlich M B, Steier P, Priller A, Revay Z, Stieghorst C, Koester U, Soldner T, Jenke T (2020)  $^{235}\text{U}(\text{n},\gamma)$  at thermal and sub-thermal energies. Consultants Meeting on Neutron Data Standards, IAEA Headquarters, Vienna, Austria (virtual meeting), 12-16 Oct 2020 <https://www-nds.iaea.org/index-meeting-crp/CM-NDS-2020-10>
67. Denecke B (1994) Absolute activity measurements with the windowless  $4\pi$ -CsI(Tl)-sandwich spectrometer. *Nucl Instrum Meth A* 339:92-98
68. Pommé S (2015) The uncertainty of counting at a defined solid angle. *Metrologia* 52:S73-S85
69. Pommé S, Johansson L, Sibbens G, Denecke B (2001) A new algorithm for the solid angle calculation applied in alpha-particle counting. Internal Report IRMM (JRC), GE/R/RN/08/2001, pp.33
70. Marouli M, Pommé S (2019) Automated optical distance measurements for counting at a defined solid angle. *Appl Radiat Isot* 153:108821
71. Pommé S (2004) A complete series expansion of Ruby's solid-angle formula. *Nucl Instr Meth A* 531:616-620
72. Pommé S, Paepen J (2007) A series expansion of Conway's generalised solid-angle formulas. *Nucl Instrum Methods A* 579:272-274
73. Pommé S (2007) The solid angle subtended by a circular detector for a linear source. *Appl Radiat Isot* 65:724-727
74. Pommé S (2007) Comments on "A comparison of different analytical methods of determining the solid angle of a circular coaxial source-detector system". *Appl Radiat Isot* 65:1065-1069
75. Pommé S, Johansson L, Sibbens G, Denecke B (2003) An algorithm for the solid angle calculation applied in alpha-particle counting. *Nucl Instrum Meth A* 505:286-289
76. Sibbens G, Pommé S, Johansson L, Denecke B (2003) Tailoring solid angle calculations to the actual radioactivity distribution of planar sources *Nucl Instrum Meth A* 505:277-281
77. Sibbens G, Pommé S, Altzitzoglou T (2004) Standardisation of low-activity actinide solutions by alpha-particle counting at a defined solid angle. *Appl Radiat Isot* 61:405-408
78. Pommé S, Altzitzoglou T, Van Ammel R, Sibbens G, Eykens R, Richter S, Camps J, Kossert K, Janßen H, García-Toráño E, Durán T, Jaubert F (2009) Experimental determination of the  $^{233}\text{U}$  half-life. *Metrologia* 46:389-456
79. M. Marouli, S. Pommé, V. Jobbagy, H. Stroh, R. Van Ammel, A. Frankhauser, R. Jakopic, S. Richter, Y. Aregbe, M. Crozet, C. Maillard, C. Rivier, D. Roudil (2020) Absolute and relative measurement of the  $^{243}\text{Am}$  half-life. *J Radioanal Nucl Chem* 326:1785-1793
80. Pommé S, Marouli M, Suliman G, Dikmen H, Van Ammel R, Jobbág V, Dirican A, Stroh H, Paepen J, Bruchertseifer F, Apostolidis C, Morgenstern A (2012) Measurement of the  $^{225}\text{Ac}$  half-life. *Appl Radiat Isot* 70:2608-2614
81. Pommé S, Altzitzoglou T, Van Ammel R, Suliman G, Marouli M, Jobbág V, Paepen J, Stroh H, Apostolidis C, Abbas K, Morgenstern A (2012) Measurement of the  $^{230}\text{U}$  half-life. *Appl Radiat Isot* 70:1900-1906
82. Ratel G (2008) Analysis of the results of the international comparison of activity measurements of a solution of  $^{55}\text{Fe}$ . *Appl Radiat Isot* 66:729-732
83. Van Ammel R, Pommé S, Sibbens G (2006) Half-life measurement of  $^{55}\text{Fe}$ . *Appl Radiat Isot* 64 (2006) 1412-1416
84. Denecke B, Bambynek W, Grosse G, Wätjen U, Ballaux C (1990) A set of X-ray fluorescence reference sources for the intrinsic efficiency calibration of Si(Li) detectors down to 1 keV. *Nucl Instrum Meth B* 49:152-156
85. Denecke B, Grosse G, Wätjen U, Bambynek W, Ballaux, C (1990) Efficiency calibration of Si(Li) detectors with X-ray reference sources at energies between 1 and 5 keV. *Nucl Instrum Meth A* 286:474-479

86. Broda R, Cassette P, Kossert K (2007) Radionuclide metrology using liquid scintillation counting. *Metrologia* 44:S36-S52
87. Kossert K, Broda R, Cassette P, Ratel G, Zimmerman B (2015) Uncertainty determination for activity measurements by means of the TDCR method and the CIEMAT/NIST efficiency tracing technique. *Metrologia* 52:S172-S190
88. Altzitzoglou T., Evaluation of the 2016 ENV57 MetroERM measurement comparison on  $^{137}\text{Cs}$ ,  $^{134}\text{Cs}$  and  $^{131}\text{I}$  in air filters. *Appl Radiat Isot* 143:123-131
89. Zimmerman B E, et al (2012) Results of an international comparison for the activity measurement of  $^{177}\text{Lu}$ . *Appl Radiat Isot* 70:1825-1830
90. Michotte C, Ratel R, Courte S, Johansson L, Keightley J, Arinc A, Bakhshandehiar E, Pommé S, Altzitzoglou T, Paepen J, Van Ammel R (2014) BIPM comparison BIPM.RI(II)-K1.Lu-177 of activity measurements of the radionuclide  $^{177}\text{Lu}$  for the NPL (UK) and the IRMM (EU), with linked results for the comparison CCRI(II)-K2.Lu-177. *Metrologia* 51:Technical Supplement 06002, 1-15
91. Pommé S, Paepen J, Van Ammel R (2018) Linearity check of an ionisation chamber through  $^{99\text{m}}\text{Tc}$  half-life measurements. *Appl. Radiat. Isot.* 140:171-178
92. Decay Data Evaluation Project (2004-2022) DDEP Monographie BIPM-5—Table of Radionuclides <http://www.lnhb.fr/nuclear-data/nuclear-data-table>
93. Nuclear Data Sheets, <https://www.journals.elsevier.com/nuclear-data-sheets>
94. Pommé S, Hardeman F, Robouch P, Etxebarria N, De Corte F, De Wispelaere A, Van Sluijs R, Simonits A (1996) General activation and decay formulas and their application in neutron activation analysis with  $k_0$  standardization. *Anal Chem* 68:4326-4334
95. Pommé S (2015) The uncertainty of the half-life. *Metrologia* 52:S51-S65
96. Pommé S (2007) Problems with the uncertainty budget of half-life measurements. Applied Modeling and Computations in Nuclear Science. T.M. Semkow, S.Pommé, S.M. Jerome, and D. J. Strom, Eds. ACS Symposium Series 945. American Chemical Society, Washington, DC, 2007, ISBN 0-8412-3982-7, 282-292
97. Pommé S, Camps J, Van Ammel R, Paepen J (2008) Protocol for uncertainty assessment of half-lives. *J Radioanal Nucl Chem* 276:335-339
98. Pommé S, De Hauwere T (2020) Derivation of an uncertainty propagation factor for half-life determinations. *Appl Radiat Isot* 158:109046
99. Pommé S, Pelczar K (2021) Empirical decomposition and error propagation of medium-term instabilities in half-life determinations. *Metrologia* 58:035012
100. Kajan I, Pommé S, Pelczar K, Heinitz S, Measurement of the  $^{145}\text{Sm}$  half-life. *Appl Radiat Isot* 178 (2021) 109978 (pp. 8)
101. Kajan I, Pommé S, Heinitz S (2022) Measurement of the  $^{171}\text{Tm}$  half-life. *J Radioanal Nucl Chem* 331:645-653
102. Van Ammel R, Pommé S, Sibbens G (2004) Experimental verification of the half-life of  $^{65}\text{Zn}$ . *Appl Radiat Isot* 60:337-339
103. Paepen J, Altzitzoglou T, Van Ammel R, Sibbens G, Pommé S (2010) Half-life measurement of  $^{124}\text{Sb}$ . *Appl Radiat Isot* 68:1555-1560
104. Van Ammel R, Paepen J, Pommé S, Sibbens G (2010) Measurement of the  $^{54}\text{Mn}$  half-life. *Appl Radiat Isot* 68:2387-2392
105. Van Ammel, Pommé S, Paepen J, Sibbens G (2011) Measurement of the  $^{109}\text{Cd}$  half-life. *Appl Radiat Isot* 69:785-789
106. Pommé S, Paepen J, Altzitzoglou T, Van Ammel R, Yeltepe E (2011) Measurement of the  $^{177}\text{Lu}$  half-life. *Appl Radiat Isot* 69:1267-1273
107. Pommé S, Suliman G, Marouli M, Van Ammel R, Jobbágy V, Paepen J, Stroh H, Apostolidis C, Abbas K, Morgenstern (2012) A measurement of the  $^{226}\text{Th}$  and  $^{222}\text{Ra}$  half-lives. *Appl Radiat Isot* 70:1913-1918

108. Pommé S, Stroh H, Benedik L (2015) Confirmation of 200% error in the  $^{209}\text{Po}$  half-life. *Appl Radiat Isot* 97:84-86
109. Collins S M, Pommé S G, Jerome S M, Ferreira K M, Regan P H, Pearce A K (2015) The half-life of  $^{227}\text{Th}$  by direct and indirect measurements. *Appl Radiat Isot* 104:203-211
110. Pommé S, Benedik L (2016) On the  $^{209}\text{Po}$  half-life error and its confirmation: an answer to the critique. *J Radiaonal Nucl Chem* 309:931-940
111. Fenwick A J, Ferreira K M, Collins S M (2016) Measurement of the  $^{109}\text{Cd}$  half-life. *Appl Radiat Isot* 109:151-153
112. Kossett K (2020) TDCR measurements to determine the half-life of  $^{55}\text{Fe}$ . *Appl Radiat Isot* 155:108931
113. Suliman G, Pommé S, Marouli M, Van Ammel R, Jobbág V, Paepen J, Stroh H, Apostolidis C, Abbas K, Morgenstern A (2012) Measurements of the half-life of  $^{214}\text{Po}$  and  $^{218}\text{Rn}$  using digital electronics. *Appl Radiat Isot* 70:1907-1912
114. Pommé S, Pelczar K, Kajan I, Verheyen L (2023) Ambient humidity, the overlooked influencer of radioactivity measurements. To be published
115. Pommé S, Keightley J (2007) Count rate estimation of a Poisson process: unbiased fit versus central moment analysis of time interval spectra. *Applied Modeling and Computations in Nuclear Science*. Semkow T M, Pommé S, Jerome S M, and Strom D J, Eds. ACS Symposium Series 945. American Chemical Society, Washington, DC, 2007, ISBN 0-8412-3982-7, 2007 pp. 316-334
116. García-Toraño E, et al (2018) The half-life of  $^{129}\text{I}$ . *Appl Radiat Isot* 140:157-162
117. García-Toraño E. (2015) Results of the EURAMET.RI(II)-S6.I-129 Supplementary Comparison. *Metrologia* 52 Techn. Suppl. 06017:1-16
118. Bé M-M, et al (2015) Determination of the  $^{151}\text{Sm}$  half-life. *Radiochimica Acta* 103:619-626
119. Bé M-M (2015) Results of the EURAMET.RI(II)-S7.Sm-151 Supplementary Comparison (EURAMET Project 1292). *Metrologia* 52 Techn. Suppl. 06016:1-18
120. Jakopic R, et al (2021)  $^{243}\text{Am}$  certified reference material for mass spectrometry. *J Radioanal Nucl Chem* 327:495-504
121. Pommé S, García-Toraño E, Sibbens G, Richter S, Wellum R, Stolarz A, Alonso A (2008)  $^{234}\text{U}/^{235}\text{U}$  activity ratios as a probe for the  $^{238}\text{U}/^{235}\text{U}$  half-life ratio. *J Radioanal Nucl Chem* 277:207-210
122. Pommé S (2015) Typical uncertainties in alpha-particle spectrometry. *Metrologia* 52:S146-S155
123. García-Toraño E (2006) Current status of alpha-particle spectrometry. *Appl Radiat Isot* 64:1273-1280
124. Crespo M T (2012) A review of electrodeposition methods for the preparation of alpha-radiation sources *Appl Radiat Isot* 70:210-215
125. Pommé S, Sibbens G (2004) Concept for an off-line gain stabilisation method. *Appl Radiat Isot* 60:151-154
126. Pommé S, Sibbens G (2004) A new off-line gain stabilisation method applied to alpha-particle spectrometry. In: Ciarlini P, Cox MG, Pavese F, Rossi GB (eds) *Advanced Mathematical and Computational Tools in Metrology VI*, Series on Advances in Mathematics for Applied Sciences – Vol. 66 (World Scientific Publishing Company) pp. 327–329
127. Paepen J, Dirican A, Marouli M, Pommé S, Van Ammel R, Stroh H (2014) A magnet system for the suppression of conversion electrons in alpha spectrometry. *Appl Radiat Isot* 87:320-324
128. Pommé S, Marroyo BC (2015) Improved peak shape fitting in alpha spectra. *Appl Radiat Isot* 96:148-153
129. Semkow T, Khan A J, Haines D K, Bari A, Sibbens G, Pommé S, Beach S, AlMahamid I, Beach G (2010) *Alpha-Spectrometry of Thick Samples for Environmental and Bioassay Monitoring*. Nuclear energy and the environment. Chien M Wai, Bruce J Mincher, Eds., ACS Symposium Series 1046, Chapter 14. American Chemical Society, Washington, DC, 2010, ISBN 9780841225855, pp. 169-177

130. García-Toraño, M.T. Crespo, M. Roteta, G. Sibbens, S. Pommé, A. Martín Sánchez, M. P. Rubio Montero, S. Woods, A. Pearce (2005) Alpha-Particle Emission Probabilities in the Decay of  $^{235}\text{U}$ . *Nucl Instr Meth* A550:581-592
131. Sibbens G, Pommé S (2004) Study of alpha-particle emission probabilities and energies in the decay of  $^{240}\text{Pu}$ . *Appl Radiat Isot* 60:155-158
132. Sibbens G, et al (2010) Alpha-particle emission probabilities in the decay of  $^{240}\text{Pu}$ . *Appl Radiat Isot* 68:1459-1466
133. Pommé S, García-Toraño E, Marouli M, Crespo T, Jobbágy V, Van Ammel R, Paepen J, Stroh H (2014) High-resolution alpha-particle spectrometry of  $^{238}\text{U}$ . *Appl. Radiat. Isot.* 87:315-319
134. Marouli M, Pommé S, Paepen J, Van Ammel R, Jobbágy V, Dirican A, Suliman G, Stroh H, Apostolidis C, Abbas K, Morgenstern A (2012) High-resolution alpha-particle spectrometry of the  $^{230}\text{U}$  decay series. *Appl Radiat Isot* 70:2270-2274
135. Marouli M, Pommé S, Jobbágy V, Van Ammel R, Paepen J, Stroh H, Benedik L (2014) Alpha-particle emission probabilities of  $^{236}\text{U}$  obtained by alpha spectrometry. *Appl Radiat Isot* 87:292-296
136. Marouli M, Pommé S, Van Ammel R, García-Toraño E, Crespo T, Pierre S (2017) Direct measurement of alpha emission probabilities in the decay of  $^{226}\text{Ra}$ . *Appl Radiat Isot* 125:196-202
137. García-Toraño E, Crespo T, Marouli M, Jobbágy V, Pommé S, Ivanov P (2019) Alpha-particle emission probabilities of  $^{231}\text{Pa}$  derived from first semiconductor spectrometric measurements. *Appl Rad Isot* 154:108863
138. Pommé S, et al (2014) Lessons Learned From Nuclear Decay Data measurements in the European Metrology Research Programme 'MetroFission'. *IEEE Transactions on Nuclear Science* 61:2066-2070
139. Spasova Y, Pommé S, Benedik L, Wätjen U (2007) Uncertainty budget for  $^{226}\text{Ra}$  activity concentration in water by alpha spectrometry. *Acta Chim Slov* 54:854-858
140. Spasova Y, Benedik L, Vasile M, Wätjen U, Pommé S (2009)  $^{234}\text{U}$  and  $^{238}\text{U}$  in drinking water – reference value and uncertainty evaluation in the frame of an interlaboratory comparison. *J Radioanal Nucl Chem* 281:113-117
141. Siegbahn K. (Editor) (1965) Alpha-, beta- and gamma-ray spectroscopy, North-Holland Publ. Co., Amsterdam, 167-172
142. Yoon W S, Kang C S, Kim S R, Kim G B, Lee H J, Lee M K, Lee J H, So J H, Kim Y H (2015) Development of a high resolution alpha spectrometer using a magnetic calorimeter. *Nucl Instr Meth A* 784:143-146
143. García-Toraño E (2018) Concept design of a time-of-flight spectrometer for the measurement of the energy of alpha particles. *Appl Radiat Isot* 134:219-224
144. Pelczar K, Pommé S (2022) Status of A-TOF Exploratory Research Project. JRC Technical Report EUR 30012 EN Publications Office of the European Union, Luxembourg, 2022, JRC128753
145. Peräjärvi K, Turunen J, Ihantola S, Kämäräinen V, Pommé S, Pöllänen R, Siiskonen T, Sipilä H, Toivonen H (2014) Feasibility of conversion electron spectrometry using a Peltier-cooled silicon drift detector. *J Radioanal Nucl Chem* 299:229-234
146. S. Pommé, J. Paepen, K. Peräjärvi, J. Turunen, R. Pöllänen (2016) Conversion electron spectrometry of Pu isotopes with a silicon drift detector. *Appl Radiat Isot* 109:183-188
147. Pommé S, Marouli M, Paepen J, Marković N, Pöllänen R (2018) Deconvolution of  $^{238,239,240}\text{Pu}$  conversion electron spectra from a silicon drift detector. *Appl Radiat Isot* 134:233-239
148. Pommé S, Paepen J, Marouli M (2019) Conversion electron spectroscopy of the 59.54 keV transition in  $^{241}\text{Am}$  alpha decay. *Appl. Radiat. Isot.* 153:108848
149. Lützenkirchen K et al. (2019) Analytical science of Plutonium. In: "Plutonium handbook – Volume 4: Chemistry", Eds. D. L. Clark, D. A. Geeson, R. J. Hanrahan Jr., American Nuclear Society, 2019, pp. 1808-1978. <http://www.ans.org/pubs/handbooks/plutonium/>
150. Sibbens G, Pommé S, Van Ammel R (2006) Total activity and Pu-238/Pu-239+240 ratio by alpha-particle counting and spectrometry for NUSIMEP-5. Internal Report IRMM, GE/RIM/01/06 (pp 21)

151. Lépy M C, et al (2001) Intercomparison for efficiency transfer software for gamma-ray spectrometry. *Appl Radiat Isot* 55:493-503
152. Maringer F J, et al (2017) Advancements in NORM metrology - Results and impact of the European joint research project MetroNORM. *Appl Radiat Isot* 126:273-278
153. Marouli M, et al (2018) Measurement of absolute  $\gamma$ -ray emission probabilities in the decay of  $^{235}\text{U}$ . *Appl Radiat Isot* 132:72-78
154. Bé M-M (2010) International exercise on  $^{124}\text{Sb}$  photon emission determination. *Appl Radiat Isot* 68:2026-2030
155. Marouli M (2019) Measurement of absolute  $\gamma$ -ray emission probabilities in the decay of  $^{227}\text{Ac}$  in equilibrium with its progeny. *Appl Radiat Isot* 144:34-46
156. Hult M, Andreotti E, González de Orduña R, Pommé S, Yeltepe E (2012) Quantification of uranium-238 in environmental samples using gamma-ray spectrometry. *EPJ Web of Conferences* 24, 07005, DOI: 10.1051/epjconf/20122407005
157. Johansson L, et al (2014) Metrology for new generation nuclear power plants – MetroFission. *IEEE Transactions on Nuclear Science* 61:2017-2023
158. Simonelli F, Abbas K, Bulgheroni A, Pommé S, Altzitzoglou T, Suliman G (2012) Measurement of the  $^{\text{nat}}\text{Hf}(\text{d},\text{x})^{177}\text{Ta}$  cross section and impact of erroneous gamma-ray intensities. *Nucl Instr Meth B* 285:162-164
159. Wallner A, et al (2020)  $^{235}\text{U}(\text{n},\gamma)$  at thermal and sub-thermal energies. Consultants Meeting on Neutron Data Standards, IAEA Headquarters, Vienna, Austria (virtual meeting), 12-16 Oct 2020; <https://www-nds.iaea.org/index-meeting-crp/CM-NDS-2020-10/>
160. Pommé S, Wagemans C, Verhaegen F, Van Den Durpel L, Van Gils J, Barthélémy R (1995) A double  $\Delta E-E$  detection set-up for ternary fission. *Nucl. Instr. and Meth. A* 359:587-595
161. Pommé S, Wagemans C (1995) Ternary-to-binary fission ratios in the resonances for  $^{235}\text{U}(\text{n},\text{f})$ . *Nucl Phys A* 587:1-12
162. De Corte F (1987) The  $k_0$ -standardization method, a move to the optimization of neutron activation analysis. *Habilitation Thesis, University of Gent, Belgium*
163. Pommé S (1999) On the applicability of  $k_0$ -NAA in extreme conditions. Ph.D. in Nuclear Chemistry, Ghent University (270 pages)
164. Pommé S, Simonits A, De Corte F, Robouch P, Hardeman F (1997) Method for the Determination of Neutron Field Monitor Burnup Effects by Gamma-spectrometry. *Anal Comm* 34:133-135
165. Pommé S, Simonits A, Lindstrom R, De Corte F, Robouch P (2000) Determination of burnup effects in  $^{197}\text{Au}(\text{n},\gamma)^{198}\text{Au}$  prior to reactor neutron field characterisation. *J Radioanal Nucl Chem* 245:223-227
166. Pommé S, Hardeman F, Robouch P, Etxebarria N (1997) Neutron Activation Analysis with  $k_0$ -standardisation : General Formalism and Procedure. Internal Report SCK-CEN, BLG 700
167. Robouch P, Eguskiza M, Maguregui M I, Pommé S, Pauwels J (2001)  $k_0$ -NAA, a valuable tool for Reference Material Producers. *Fresenius J Anal Chem* 370:255-258
168. Robouch P, Arana G, Eguskiza M, Maguregui M I, Pommé S, Ingelbrecht C (2002) Target preparation and neutron activation analysis: a successful story at IRMM. *Nucl Instr Meth A* 480:128-132
169. Uyttenhove J, Pommé S, Van Waeyenberge B, Hardeman F, Buysse J, Culot J-P (1997) Survey of the  $^{137}\text{Cs}$  Contamination in Belgium by In-Situ Gamma Spectrometry, A Decade after the Chernobyl Accident. *Health Physics* 73:644-646
170. Pommé S, Uyttenhove J, Van Waeyenberge B, Genicot J-L, Culot J-P, Hardeman F (1998) Radiocesium Contamination in Belgium. *J Radioanal Nucl Chem* 235:139-144
171. Genicot J-L, Pommé S (1999) Attenuation Calculation of Low Energy Photons: Application to In-Vivo Spectrometry using Multi-Diode Systems. *Rad Prot Dosim* 81:113-122

172. Genicot J-L, Pommé S, Alzetta J-P (1999) In-Vivo Measurement of Low Energy Photon Emitters: Room-Temperature Semiconductor Diodes vs. Large Scintillators and Germanium Crystals. *Health Physics* 76:288-299
173. Robouch P, Arana G, Eguskiza M, Pommé S, Etxebarria N (2000) Uncertainty budgets for  $k_0$ -NAA. *J Radioanal Nucl Chem* 245:195-197
174. Pommé S, Hardeman F, Etxebarria N, Robouch P (1997) Performance Optimization of  $k_0$ -INAA. *J Radioanal Nucl Chem* 215:295-303
175. Van Lierde S, De Corte F, Bossus D, van Sluijs R, Pommé S (1999) Determination of  $k_0$  and related nuclear data for short-lived radionuclides to be used in KAYZERO-NAA at DSM Research. *Nucl Instr Meth A* 422:874-879
176. De Corte F, Van Lierde S, Simonits A, Bossus D, van Sluijs R, Pommé S (1999) A re-evaluation of  $k_0$  and related nuclear data for the 555.8 keV gamma-line emitted by the  $^{104m}\text{Rh}$ - $^{104}\text{Rh}$  mother-daughter pair. *Appl Rad Isot* 51:701-706
177. Simonits A, De Corte F, Van Lierde S, Pommé S, Robouch P, Eguskiza M (2000) The  $k_0$  and  $Q_0$  values for the Zr-isotopes : a re-investigation. *J Radioanal Nucl Chem* 245:199-203
178. Verboven M, Jacobs E, Piessens M, Pommé S, De Frenne D, De Clercq A (1990) Fragment mass and kinetic energy distributions for the photofission of  $^{234}\text{U}$  with 12-, 15- and 20-MeV bremsstrahlung. *Phys Rev C* 42:453-456
179. Arruda-Neto J D T, Jacobs E, De Frenne D, Pommé S (1990) Evidence for isomeric electron induced fission of  $^{232}\text{Th}$ . *Phys Lett B* 248:34-38
180. Piessens M, Jacobs E, Pommé S, De Frenne D (1993) Mass and Kinetic Energy Distributions for the Photofission of  $^{232}\text{Th}$  with 6.44 to 13.15 MeV bremsstrahlung. *Nucl Phys A* 556:88-106
181. Pommé S, Jacobs E, Piessens M, De Frenne D, Persyn K, Govaert K, Yoneama M-L (1994) Fragment characteristics for the photofission of  $^{238}\text{U}$  with 6.1-13.1 MeV bremsstrahlung. *Nucl Phys A* 572:237-266
182. Wagemans C, Demattè L, Pommé S, Schillebeeckx P (1996) Mass and Energy Distributions for  $^{243}\text{Am}(n_{th},f)$ . *Nucl Phys A* 579:188-196
183. Yoneama M-L et al. (1996) Study of the  $^{232}\text{Th}$  fission barrier by electron-induced fission. *Nucl Phys A* 604:263-284
184. Persyn K, Jacobs E, Pommé S, De Frenne D, Govaert K, Yoneama M-L (1997) Excitation energy dependence of fragment characteristics for the photofission of  $^{232}\text{Th}$ . *Nucl Phys A* 620:171-190
185. Pommé S (1992) Massa-, ladings- en energiedistributies voor  $^{238}\text{U}(\gamma^*,f)$  in het barrièregebied. Ph.D. in Nuclear Physics, Ghent University
186. Pommé S, Jacobs E, Persyn K, De Frenne D, Govaert K, Yoneama M-L (1993) Excitation energy dependence of charge odd-even effects in the fission of  $^{238}\text{U}$  close to the fission barrier. *Nucl. Phys. A* 560:689-714
187. Persyn K, Jacobs E, Pommé S, De Frenne D, Govaert L, Yoneama M-L (1997) Influence of the odd neutron on the fragment characteristics in the photofission of  $^{235}\text{U}$ . *Nucl. Phys. A* 615:198-206
188. Govaert K et al. (1994) Polarised Bremsstrahlung Nuclear Resonance Fluorescence Set-up at the 15-MeV Linac in Gent. *Nucl Instr Meth A* 337:265-273
189. Mondelaers W, Van Laere K, Goedefroot A, Van den Bossche K (1996) The Gent University 15 MeV high-current linear electron accelerator facility. *Nucl Instr Meth A* 368:278-282
190. Piessens M, Jacobs E, Pommé S, De Frenne D (1993) Range of  $^{232}\text{Th}(\gamma,f)$  fragments in metallic Th. *Nucl Instr Meth B* 82:7-8
191. Rutherford E (1900) A radio-active substance emitted from thorium compounds. *Phil Mag S 5 Vol 49 No 296*
192. Pommé S et al (2018) Is decay constant? *Appl Radiat Isot* 134:6-12

193. McDuffie M H, Graham P, Eppele J L, Gruenwald J T, Javorsek II D, Krause D E, Fischbach E (2020) Anomalies in radioactive decay rates: A bibliography of measurements and theory. Preprint at <https://arxiv.org/abs/2012.00153>
194. Pommé S et al (2016) Evidence against solar influence on nuclear decay constants. *Phys Lett B* 761:281–286
195. Pommé S et al (2017) On decay constants and orbital distance to the Sun—part I: alpha decay. *Metrologia* 54:1–18
196. Pommé S et al (2017) On decay constants and orbital distance to the Sun—part II: beta minus decay. *Metrologia* 54:19–35
197. Pommé S et al (2017) On decay constants and orbital distance to the Sun— part III: beta plus and electron capture decay. *Metrologia* 54:36–50
198. Pommé S, Kossert K, Nähle O (2017) On the claim of modulations in  $^{36}\text{Cl}$  beta decay and their association with solar rotation. *Solar Phys* 292:162
199. Pommé S, Lutter G, Marouli M, Kossert K, Nähle O (2017) On the claim of modulations in radon decay and their association with solar rotation. *Astropart Phys* 97:38–45
200. Pommé S, Lutter G, Marouli M, Kossert K, Nähle O (2018) A reply to the rebuttal by Sturrock et al. *Astropart Phys* 107:22–25
201. Pommé S (2019) Solar influence on radon decay rates: irradiance or neutrinos? *Eur Phys J C* 79:73
202. Pommé S, Pelczar K (2020) On the recent claim of correlation between radioactive decay rates and space weather. *Eur Phys J C* 80:1093
203. Pommé S, Pelczar K, Kossert K, Kajan I (2021) On the interpretation of annual oscillations in  $^{32}\text{Si}$  and  $^{36}\text{Cl}$  decay rate measurements. *Sci Rep* 11:16002
204. S. Pommé, T. De Hauwere (2020) On the significance of modulations in time series. *Nucl Instr Meth A* 956:163377
205. Pommé S, Pelczar K (2022) Role of ambient humidity underestimated in research on correlation between radioactive decay rates and space weather. *Sci Rep* 12:2527
206. Pommé S, Pelczar K, Kajan I (2022) Air humidity and annual oscillations in  $^{90}\text{Sr}/^{90}\text{Y}$  and  $^{60}\text{Co}$  decay rate measurements. *Sci Rep* 12:9535
207. Sagan, C (1995) The demon-haunted world: science as a candle in the dark (Random House)
208. Schrader H (2010) Half-life measurements of long-lived radionuclides – New data analysis and systematic effects. *Appl Radiat Isot* 68:1583–1590
209. Pommé S, et al. Ambient humidity, the overlooked influencer of radioactivity measurements. To be published
210. Weather Underground, Antwerp International Airport Station, Antwerp, Belgium, Weather History, Website: <https://www.wunderground.com/history/monthly/be/antwerp/EBAW/date/2022-1>
211. S. Pommé (2020) Comparing significance criteria for cyclic modulations in time series. *Nucl Instr Meth A* 968:163933
212. Rovelli C (2017) Reality is not what it seems. Penguin Books Ltd.
213. Rovelli C (2019) The order of time. Penguin Books Ltd.
214. Pommé S, Jerome S, Venchiarutti C (2014) Uncertainty propagation in nuclear forensics. *Appl Radiat Isot* 89:58–64
215. Pommé S, Collins S (2014) Unbiased equations for  $^{95}\text{Zr}-^{95}\text{Nb}$  chronometry. *Appl Radiat Isot* 90:234–240
216. Pommé S, Collins S M, Harms A V, Jerome S M (2016) Fundamental uncertainty equations for nuclear dating applied to the  $^{140}\text{Ba}-^{140}\text{La}$  and  $^{227}\text{Th}-^{223}\text{Ra}$  chronometers. *J. Env Radioact* 162–163:358–370
217. Pommé S, et al. Calibration of an ionisation chamber for parent-progeny decay. To be published

218. Pommé S Dead time, pile-up and statistics. Applied Modeling and Computations in Nuclear Science. Semkow T M, Pommé S, Jerome S M, and Strom D J, Eds. ACS Symposium Series 945. American Chemical Society, Washington, DC, 2007, ISBN 0-8412-3982-7, 2007 pp. 218-233
219. Pommé S (1998) Time distortion of a Poisson process and its effect on experimental uncertainty. *Appl Radiat Isot* 49:1213-1218
220. Pommé S, Denecke B, Alzetta J-P (1999) Influence of pileup rejection on nuclear counting, viewed from the time-domain perspective. *Nucl Instr Meth A* 426:564-582
221. Pommé S (1999) Time-interval distributions and counting statistics with a non-paralysable spectrometer. *Nucl Instr Meth A* 437:481-489
222. Pommé S, Uyttenhove J (2001) Statistical precision of high-rate spectrometry with a Wilkinson ADC. *J Radioanal Nucl Chem* 248:263-266
223. Pommé S (2008) Cascades of pile-up and dead time. *Appl Rad Isot* 66:941-947
224. Pommé S, Kennedy G (2000) Pulse Loss and Counting Statistics with a Digital Spectrometer. *Appl Rad Isot* 52:377-380
225. Choi H D 2009 Counting statistics distorted by two dead times in series which end with an extended type dead time *Nucl. Instrum. Methods A* 599 251-9
226. Choi H D 2011 Counting statistics modified by two dead times in series *Nucl. Eng. Technol.* 43 287-300
227. Müller J (1981) Counting statistics of short-lived nuclides. *J Radioanal Nucl Chem* 61:345-359
228. Fitzgerald R (2016) Corrections for the combined effects of decay and dead time in live-timed counting of short-lived radionuclides. *Appl Rad Isot* 109:335-340
229. Westphal G P (2008) Review of loss-free counting in nuclear spectroscopy. *J Radioanal Nucl Chem* 275:677-685
230. Heydorn K, Damsgaard E (1997) Validation of a loss-free counting system for neutron activation analysis with short-lived indicators. *J. Radioanal. Nucl. Chem.* 215:157-160
231. Pommé S (1999) How pileup rejection affects the precision of loss-free counting. *Nucl Instr Meth A* 432:456-470
232. Pommé S (1999) Is Loss-Free Counting under Statistical Control? *Biol Trace Element Res* 71-72:415-422
233. S. Pommé, J-P. Alzetta, J. Uyttenhove, B. Denecke, G. Arana, P. Robouch (1999) Accuracy and Precision of Loss-Free Counting in  $\gamma$ -ray Spectrometry. *Nucl Instr Meth A* 422:388-394
234. Pommé S, Robouch P, Arana G, Eguskiza M, Maguregui M I (2000) Is it safe to use Poisson Statistics in Nuclear Spectrometry? *J Rad Nucl Chem* 244:501-506
235. Pommé S (2001) Experimental test of the 'zero dead time' count-loss correction method on a digital gamma-ray spectrometer. *Nucl Instr Meth A* 474:245-252
236. Pommé S (2002) A plausible mathematical interpretation of the 'variance' spectra obtained with the DSPECPLUS™ digital spectrometer. *Nucl. Instr. Meth.* A482/565-566
237. Pommé S (2003) On the statistical control of 'loss-free counting' and 'zero dead time' spectrometry. *J Radioanal Nucl Chem* 257:463-466
238. Denecke B, de Jonge S (1998) An analyzer for pulse-interval times to study high-order effects in the processing of nuclear detector signals. *Appl Radiat Isot* 49:1099-1105

## 9 List of figures

Figure 1: The SIR, SIRTI, and ESIR activity transfer instruments operated by the Ionizing Radiation Department of BIPM for demonstrating equivalence of the SI-derived unit becquerel. ....	6
Figure 2: Simulation results for measures of efficiency and robustness of the arithmetic (AM), Mandel–Paule (M-P), power-moderated (PMM), inverse-variance weighted (WM), and Der Simonian–Laird (D-L) mean for discrepant data sets as a function of the number of data. (Top) Standard deviation of the mean around the true value used in the simulation. (Bottom) Ratio of the standard deviation of the mean to the calculated uncertainty. The PMM is almost as robust as the AM, yet more efficient. WM, M-P and D-L underestimate the uncertainty.....	7
Figure 3: A combinatory PomPlot of a non-exhaustive set of key comparison results for activity standardisations of radionuclides, through the SIR (K1) and direct comparisons (K2). Several inconsistent data are due to the difficult standardisation of $^{125}\text{I}$ . Overall, the uncertainties in the last two decades have been somewhat more homogenous and realistic than in the past (see Fig. 4 in [25] for comparison). ....	8
Figure 4: Fishing of a gold-evaporated VYNS foil on a large support ring, after it was soaked off a glass plate in the water bath. Upon drying, the wrinkles in the foil straighten out. ....	10
Figure 5: Design of JRC's large pressurised proportional counter (LPPC). There is a choice of cathodes with a cut-out of 35 mm or 56 mm diameter to accommodate standard (34 mm) or large (55 mm) source substrates, respectively. The source support is a metal ring covered with a gold-coated VYNS foil; a clamp keeps it firmly in position.....	11
Figure 6: Dr. Stefaan Pommé and visiting scientist Dr. Hasan Dikmen inspecting the classical electronics used for coincidence counting.....	12
Figure 7: Technical drawing of the small pressurised proportional counter (SPPC), showing the dimensions of the source support, the cathode acting as source holder, and the gas counter with two anode wires.....	13
Figure 8: Drawing of the NaI(Tl) well detector used in the $4\pi \beta\gamma$ coincidence (and sum) counting method, when it hosts the SPPC in the well. It is also used standalone for $4\pi \gamma$ counting. ....	13
Figure 9: Technical drawing of the NaI(Tl) well detector specifically designed for the $4\pi \gamma$ counting method. It can also be used for $4\pi \beta\gamma$ coincidence counting when inserting plastic scintillators and a slender photomultiplier tube into the well. ....	14
Figure 10: Drawing of the CsI(Tl) sandwich spectrometer and the source-interlock chamber. The source support (top right) is a VYNS foil covering a 10-mm-diameter hole in a 3.2- $\mu\text{m}$ -thick mylar foil pressed between solid brass rings. ....	15
Figure 11: Dr Maria Marouli optically measuring the thickness of a source using a vertically traveling microscope with distance probe, which is currently replaced by a 3D-coordinate measuring machine [70]....	16
Figure 12: Drawing of one of the x ray DSA counters consisting of two source chambers separated by a distance tube, a diaphragm, and a gas proportional counter with a 25- $\mu\text{m}$ -thick berillium entrance window. 17	17
Figure 13: Dr. Timotheos Altzitzoglou and visiting scientist Dr. Gülen Ozçyn operating an ultra-low background liquid scintillation spectrometer.....	18
Figure 14: PomPlots of CCRI(II) K2 key comparisons of activity. The radionuclides and the year of execution are indicated in the corner of the graphs. The red dots represent the JRC results. In the case of $^{177}\text{Lu}$ [89,90], the JRC result at $u/S=4.5$ and $\zeta=0.6$ is off the scale due to the large uncertainty estimate. The same applies to extremely discrepant or uncertain data from other NMIs.....	19
Figure 15: Aggregate PomPlot of JRC's results in the KCs depicted in Figure 14. The distribution of the data shows that the measurements are very accurate and the stated uncertainties are reliable.....	20
Figure 16: Aggregate PomPlot of JRC's partial results with individual primary standardisation techniques. The results are mutually consistent and free of bias. ....	20

Figure 17: Top view of the ionisation chamber IC1 of the JRC (top) and front view of the IC1 in a lead brick shielding at the right, its electronics, and below the charge-integrating air capacitor in a lead shield (bottom). .....	21
Figure 18: Overview of $^{109}\text{Cd}$ half-life measurement results, their standard uncertainties, and their year of publication [105,111]. The data of 1981 and 2010 are from the JRC. The line corresponds to a mean of the three most recent values. ....	23
Figure 19: Overview of $^{55}\text{Fe}$ half-life measurements, their standard uncertainties, and their year of publication [41,112]. The data of 2006 and 2019 are from the JRC and the line corresponds to JRC's most accurate value. .....	24
Figure 20: Dr. Stefaan Pommé and visiting scientist Dr. Abdullah Dirican at the small vacuum chambers with planar silicon detectors used for measurements of half-lives in the $^{230}\text{U}$ and $^{225}\text{Ac}$ decay series, as well as $^{209}\text{Po}$ . .....	25
Figure 21: Top: Traditional peak shape model based on the convolution of a Gaussian with three exponential tailing functions. Middle: Failed peak fit to a $^{240}\text{Pu}$ alpha spectrum with very high statistical accuracy, using three tailing functions. Bottom: Fit of the same $^{240}\text{Pu}$ spectrum with the 'BEST' shaping model [128]. .....	27
Figure 22: Drs. Krzysztof Pelczar and Stefaan Pommé at the construction of the A-TOF facility, which measures the energy of alpha particles emitted in radioactive decay. The energy resolution is improved by measuring the time-of-flight of the alpha particles over a flightpath of several meters. The aim is to provide accurate nuclear decay data of alpha-emitting nuclides. ....	28
Figure 23: Visiting scientist Dr. Belén Caro Marroyo introducing a source in the conversion electron spectrometer equipped with a silicon drift detector. She co-developed the 'BEST' spectral analysis software.	29
Figure 24: Top: Model representation of mixed alpha spectra from plutonium isotopes (with low and high energy resolution) [149]. Bottom: Measured L-shell conversion electron spectrum of a mixed plutonium source and individual spectra of $^{238,239,240}\text{Pu}$ [146]. ....	30
Figure 25: Charge distribution of the heavy fission products from bremsstrahlung-induced photofission of $^{238}\text{U}$ at three average excitation energies, measured by $\gamma$ -ray spectrometry of the decay products. The odd-even effect disappears when the excitation energy supersedes the pairing gap at the fission barrier. ....	33
Figure 26: Measured fragment charge odd-even effect as a function of the average excitation energy of $^{238}\text{U}$ at the fission barrier [186]. The line represents a deconvolution of the data accounting for the continuous energy distribution of the bremsstrahlung used for excitation. The odd-even effect drops near the pairing gap at 2.2 MeV. ....	33
Figure 27: Average values and standard uncertainty of residuals to exponential decay of $^{134}\text{Cs}$ in JRC's ionisation chamber IC1 in Geel, Belgium binned as a function of ambient humidity obtained from a weather station in Antwerp at about 40 km distance [210]. Humidity causes an annual cycle in the data.....	35
Figure 28: Amplitudes of annual ( $1 \text{ a}^{-1}$ ) and monthly ( $9.43 \text{ a}^{-1}, 12.7 \text{ a}^{-1}$ ) sinusoidal cycles fitted to the residuals from exponential decay of various nuclides as a function of the uncertainty on the amplitude. The dotted lines correspond to 1% probability for outliers at the low and high side of the associated Rayleigh statistical distribution of random noise. The data were not corrected for environmental influences, which explains the presence of significant annual cycles. ....	36
Figure 29: Uncertainty propagation factors of the activity ratio and the parent and progeny half-lives towards radiochronometry for hypothetical measurements of two days. The exact formula (symbols) is compared to the classical formula (lines) in which decay during the measurement is not taken into account [216]......	38
Figure 30: The achieved statistical control over the residuals of $^{227}\text{Th}$ - $^{223}\text{Ra}$ radiochronometry results using HPGe detectors at the NPL [216]. On the x-axis is the time of measurement relative to the moment of chemical separation of $^{227}\text{Th}$ from its progeny. The y-axis shows the error of the calculated separation date through radiochronometry, which was mostly within the calculated standard uncertainty. ....	38
Figure 31: Measured and theoretical time-interval spectrum in a $\gamma$ -ray spectrometer with pileup rejection, which is the main count loss mechanism [220]. $T_w$ is the pulse width and PET the width of the rising edge of the pulse. ....	39

Figure 32: LFC techniques add virtual counts to the spectrum to compensate for count loss based on the real-time to live-time ratio in short time intervals [229]. . . . .	40
Figure 33: Left: Time-interval distributions of the full spectrum and a 30% fraction of the spectrum for counters with non-extending dead time, extending dead time, and pileup rejection. Right: Corresponding standard deviation of counting in real time, relative to Poisson uncertainty and as a function of input rate. . . . .	41
Figure 34: Broadening of the valid count distribution in a live-time period due to pileup rejection, compared to extending dead time for which Poisson statistics applies [231]. . . . .	41
Figure 35: Deviation of LFC statistical uncertainty from Poisson statistics as a function of input rate, when taking the integral number of events in the full spectrum. For small fractions of the spectrum, the Westphal formula is asymptotically valid. . . . .	42

## **GETTING IN TOUCH WITH THE EU**

### **In person**

All over the European Union there are hundreds of Europe Direct information centres. You can find the address of the centre nearest you at: [https://europa.eu/european-union/contact\\_en](https://europa.eu/european-union/contact_en)

### **On the phone or by email**

Europe Direct is a service that answers your questions about the European Union. You can contact this service:

- by freephone: 00 800 6 7 8 9 10 11 (certain operators may charge for these calls),
- at the following standard number: +32 22999696, or
- by electronic mail via: [https://europa.eu/european-union/contact\\_en](https://europa.eu/european-union/contact_en)

## **FINDING INFORMATION ABOUT THE EU**

### **Online**

Information about the European Union in all the official languages of the EU is available on the Europa website at: [https://europa.eu/european-union/index\\_en](https://europa.eu/european-union/index_en)

### **EU publications**

You can download or order free and priced EU publications from EU Bookshop at: <https://publications.europa.eu/en/publications>. Multiple copies of free publications may be obtained by contacting Europe Direct or your local information centre (see [https://europa.eu/european-union/contact\\_en](https://europa.eu/european-union/contact_en)).

**The European Commission's  
science and knowledge service**  
Joint Research Centre

**JRC Mission**

As the science and knowledge service of the European Commission, the Joint Research Centre's mission is to support EU policies with independent evidence throughout the whole policy cycle.



**EU Science Hub**  
[ec.europa.eu/jrc](http://ec.europa.eu/jrc)



@EU\_ScienceHub



EU Science Hub - Joint Research Centre



EU Science, Research and Innovation



EU Science Hub



Publications Office  
of the European Union

doi: 10.2760/666973

ISBN 978-92-76-54093-9